Journal of Hydrology 632 (2024) 130891

Contents lists available at ScienceDirect

Journal of Hydrology

journal homepage: www.elsevier.com/locate/jhydrol

Research papers

Uncertainty on flow rate and temperature measurement for the detection of illicit flows in sewers

Anita Raimondi *, Umberto Sanfilippo, Gianfranco Becciu

Department of Civil and Environmental Engineering, Politecnico di Milano, Piazza Leonardo da Vinci 32, 20133 Milano, Italy

ARTICLE INFO

This manuscript was handled by A. Bardossy, Editor-in-Chief, with the assistance of Zhenxing Zhang, Associate Editor

Keywords:
Sewers
Stormwater Runoff Management
Flood Control
Illicit Flows
Uncertainty Analysis

ABSTRACT

Sewers often undergo crucial problems because of the combined effects of urbanization and extreme rainfall events. In addition, unexpected flows drained or discharged into the network, the so-called illicit flows, can overload the drainage systems. Their presence involves several environmental problems and increases both the flood risk, and the operational costs of the wastewater treatment plants. This study investigates the performances of combining flow rate and temperature measurements to estimate illicit flows in sewer systems. The goal is to identify an optimal configuration of flow meters and temperature sensors that can enhance reliability, accuracy, and money saving. Two applications have been used to validate the proposed framework. The first is a set of significant computational examples. The second is an application to an existing sewer network in Milano (Italy) within a research project funded by Regione Lombardia. The proposed method has proved to be suitable thanks to its simplicity, adaptability, and cost-effectiveness.

1. Introduction

The urban population has been growing dramatically since the second half of the past century, and the trend does not show signs of stopping (Hoornweg and Pope, 2017); it can be estimated that it will reach about 66 % of the total population by 2050 (Habitat, 2011). This trend involves also higher and higher volumes of water demand; those volumes must be conveyed by urban fresh water supply systems to satisfy the human needs, and then are discharged into the sewer systems to be treated by the downstream wastewater treatment plants. Moreover, urbanization progressively entails soil sealing, causing an increase of stormwater runoff volumes and peaks. So, the combined sewer systems, as well as the stormwater networks of the separated systems, are often overloaded, primarily when extreme rainfalls occur. The intensification of these events is one of the main effects of climate change; in particular, the World Meteorological Organization (WMO) stated that they rise by 7 % for each degree of global temperature increase (Pall et al., 2007; Allen and Ingram, 2002).

Moreover, sewers are usually extensive and often aging structures, subject to cracks and misconnections during their operational lifetime (Sadeghikhah et al., 2023). Therefore, they can be subject to exfiltration and infiltration of illicit flows, depending on the relative position between the free water surface in the pipes and the groundwater level (Nguyen et al., 2021). Illicit flows are unexpected and unwanted waters drained from or discharged into the urban drainage systems; depending on their source, they can be distinguished into infiltrations and inflows. The first kind generally comes from aquifers or surface channels that can enter the network through broken pipes, leaky connections, or deteriorated manholes. The second kind comes from unauthorized and/or incorrect connections to the sewers.

As already said, illicit flows cause several issues in urban water management. They involve sewer overload and the related rise of flood risk (Weiß et al., 2002). They increase the activation frequency of Combined Sewer Overflows (CSOs) and the uncontrolled discharge of pollutants into the receiving water bodies (Xu et al., 2023). Illicit flows can even neutralize the benefits of green infrastructures, since the reduction of surface runoff is offset by the increase of groundwater infiltrations into the drainage system (Zhang and Parolari, 2022; Zhang et al., 2023). Moreover, they reduce flows in urban streams, especially the low flow ones during dry weather (Pangle et al., 2022). Illicit flows also affect the pumping systems, altering the design functioning and increasing energy costs (Rezaee and Tabesh, 2022). Finally, they dilute the wastewater flows entering the treatment plants, reducing the efficiency of their processes, and increasing their operational costs. The temporal pattern of illicit flows can be constant or variable; infiltrations from aquifers and surface channels primarily occur during the irrigation

* Corresponding author.
E-mail addresses: anita.raimondi@polimi.it (A. Raimondi), umberto.sanfilippo@polimi.it (U. Sanfilippo), gianfranco.becciu@polimi.it (G. Becciu).

https://doi.org/10.1016/j.jhydrol.2024.130891
Received 11 August 2023; Received in revised form 24 January 2024; Accepted 29 January 2024
Available online 15 February 2024
0022-1694/© 2024 The Author(s). Published by Elsevier B.V. This is an open access article under the CC BY license (http://creativecommons.org/licenses/by/4.0/).

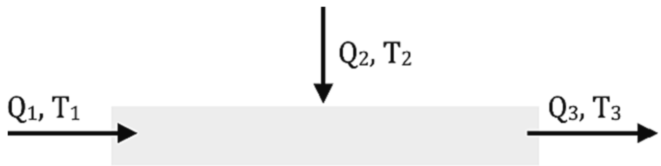

Fig. 1. Scheme of reference for the analysis. Flow rate (Q) and temperature (T) of the upstream flow (subscript 1), downstream flow (subscript 3), and illicit flow (subscript 2).

Table 1
Resolution of the system of Eq. (1) for schemes A, B, and C, Example 1.

Scheme	Known variables				Unknown variables	
A	$Q_1 = 50$ l/s	$Q_3 = 100$ l/s	$T_1 =$ 20 °C	$T_3 =$ 18 °C	$Q_2 =$ 50 l/s	$T_2 =$ 16 °C
B	$Q_3 =$ 100 l/s	$T_1 =$ 20 °C	$T_2 =$ 30 °C	$T_3 =$ 25 °C	$Q_1 =$ 50 l/s	$Q_2 = 50$ l/s
C	$Q_1 = 50$ l/s	$T_1 =$ 20 °C	$T_2 =$ 30 °C	$T_3 =$ 25 °C	$Q_2 =$ 50 l/s	$Q_3 = 100$ l/s

Table 2
Relative uncertainties in estimating illicit flow rate and temperature, Example 1.

Scheme	Measurement uncertainties	$U(Q_2)/Q_2$	$U(T_2)/T_2$
A	$U(Q_i) = 5$ %, $U(T_i) = 0.5$ °C	11 %	18 %
	$U(Q_i) = 10$ %, $U(T_i) = 1.0$ °C	22 %	37 %
B	$U(Q_i) = 5$ %, $U(T_i) = 0.5$ °C	13 %	2 %
	$U(Q_i) = 10$ %, $U(T_i) = 1.0$ °C	26 %	3 %
C	$U(Q_i) = 5$ %, $U(T_i) = 0.5$ °C	25 %	2 %
	$U(Q_i) = 10$ %, $U(T_i) = 1.0$ °C	50 %	3 %

season, while inflows are generally (but not always) intermittent and discontinuous. Their percentage can vary on time and space, depending on the rainfall regime (Panasiuk et al., 2019) and land use (Loc et al., 2022). Sometimes, illicit flows can achieve a very high percentage of the total flow in drainage systems. For example, Bentes et al. (2022) has found that 85 % of the wastewater flowing to the Folhadela WWTP (Portugal) come from illicit flows.

In many countries, regulations stress the importance of reducing illicit flows into sewers. In Italy, in this sense, the regional regulation of Regione Lombardia (R.R. March 29th, 2019, n.6) suggests limiting them to 30 % of the average annual flow during dry periods. To this aim, it is fundamental to detect illicit flows, find their sources and make quantitative evaluations of them. The scientific and technical research on illicit flows in urban sewer systems includes three main work areas (Ellis and Bertrand-Krajewski, 2010): the first is the development of new measurement methods including detailed uncertainty analyses; the second is the implementation of proper models to integrate structural and experimental data, in order to facilitate operational management and decision-making processes; the third consists in cost estimation, economic evaluation, performance indicators and multi-criteria methods applied to investment/rehabilitation strategies. The initial step for illicit flows detection is usually to identify the most critical areas and network sections, where further investigations must be developed at a local scale. To this aim, the analyses of the night-time minimum values of the dry weather flows are usually suitable. Then, several methodologies and technologies are available (Butler and Davies, 2004; Panasiuk et al., 2015); but choosing the most effective out of them depends, in practice, on the specific site conditions and the economic resource availability. Moreover, different techniques can be used in tandem to detect illicit flows, strengthening the benefits of each one (Beheshti and Saegrov, 2019). Among these, the most used in practice are visual inspections, the dye test (Zhao et al., 2020), closed-Circuit Television Camera (CCTV) inspections and Infra-Red cameras (Lepot et al., 2017), and the stable isotopes technique (Kracht et al., 2007; Prigiobbe and Giulianelli, 2009).

A quite recent technology to detect illicit flows is Distributed Temperature Sensing (DTS). Although the technique dates since the 1980 s (Ukil et al., 2012), the first application to sewer systems was in 2009 (Schilperoort and Clemens, 2009). It has been employed in different fields, from ocean to atmospheric monitoring (Hausner and Kobs, 2016), for a broad range of hydrologic processes (Selker et al., 2006) to study the interaction between water bodies (Lowry et al., 2007), to monitor sediment accumulation (Regueiro-Picallo et al., 2023), etc. DTS enables the monitoring of temperatures in various systems at much higher spatial and temporal frequencies than any previous method (Tyler et al., 2009), achieving high resolutions (Hoes et al., 2009; Kechavarzi et al., 2020). In addition, the double-ended calibration achieves accurate temperature measurements under field conditions (Van de Giesen et al., 2012). In principle, DTS continuously measures the temperature along a fiber optic cable inserted in the sewer. It can be applied on a large spatial scale, over a long period, without requiring access to private properties, enabling the detection of very infrequent anomalies (Kessili et al., 2018). Several field campaigns have confirmed the feasibility and promising applicability of DTS (Schilperoort et al., 2013; Pawlowski et al., 2014; Beheshti and Saegrov, 2018; Pangle et al., 2022). Its main limitation is that it works well only if the temperature of the illicit flow differs from that of the flow in the network (Nienhuis et al., 2013). Moreover, high spatial and temporal resolutions produce a large amount of data to be analyzed (Vosse et al., 2013). An interesting alternative to DTS consists in the simultaneous and punctual measuring of flow rates and temperatures in some strategic manholes of the network by means of temperature sensors and flow meters. The method can indicate the source of illicit flow but cannot identify the exact input point. Temperature sensors can be even combined with conductivity sensors (Schilperoort et al., 2006; Shi et al., 2022). The advantage of using flow meters is that they enable the quantification of illicit flows. The appropriate positioning of temperature sensors and flow meters is fundamental for the reliability and accuracy of the approach. To this aim, Sambito et al. (2020) proposed a Bayesian Decision Network (BDN) to locate water quality sensors in a combined sewer in Italy in the best way. Selker and Selker (2014), in a study on the effects of the location of seeps of groundwaters into surface waters, concluded that even the burial depth influences the results. In real applications, a trade-off between measurement accuracy and number, temporal and spatial resolution must be achieved (Selker et al., 2006). Moreover, the literature proposes several models to manage the large amount of data collected during field surveys, estimating, and locating the contribution of different sources of illicit flow. The Storm Water Management Model RTK method (Camp Dresser and McKee Inc. et al., 1985) makes use of three-unit hydrographs to estimate the response times associated with the effect of fast, moderate, and slow infiltration and inflow by a linear convolution. Kessili et al. (2018) developed an automated tool to analyse large data masses and identify anomalies caused by illicit flows. Tanda et al. (2023) proposed two types of inverse computational techniques (artificial neural network and Kalmar filter technique) to identify the source location of illegal inflows into wastewater systems. Xu et al. (2021) developed an inversed optimization model to diagnose and locate illicit flows through a trial-and-error method using automatic iteration to optimize its estimation. Choi and Schmidt (2023) suggested a genetic algorithm to calculate the weighting factors of the different Impulse Response Functions (IRF) associated with each source. Zhang et al. (2018) proposed a method to decompose Rainfall-Derived Inflow (RDI) and Rainfall-Induced Infiltration (RII) based on conductivity data.

Nevertheless, all the methods and technologies discussed for detecting illicit flows present some uncertainties due to the measurement tools and flow conditions (Prigiobbe and Giulianelli, 2009). This paper focuses on the combined measurements of flow rates and temperature to detect and quantify illicit waters in sewer systems.

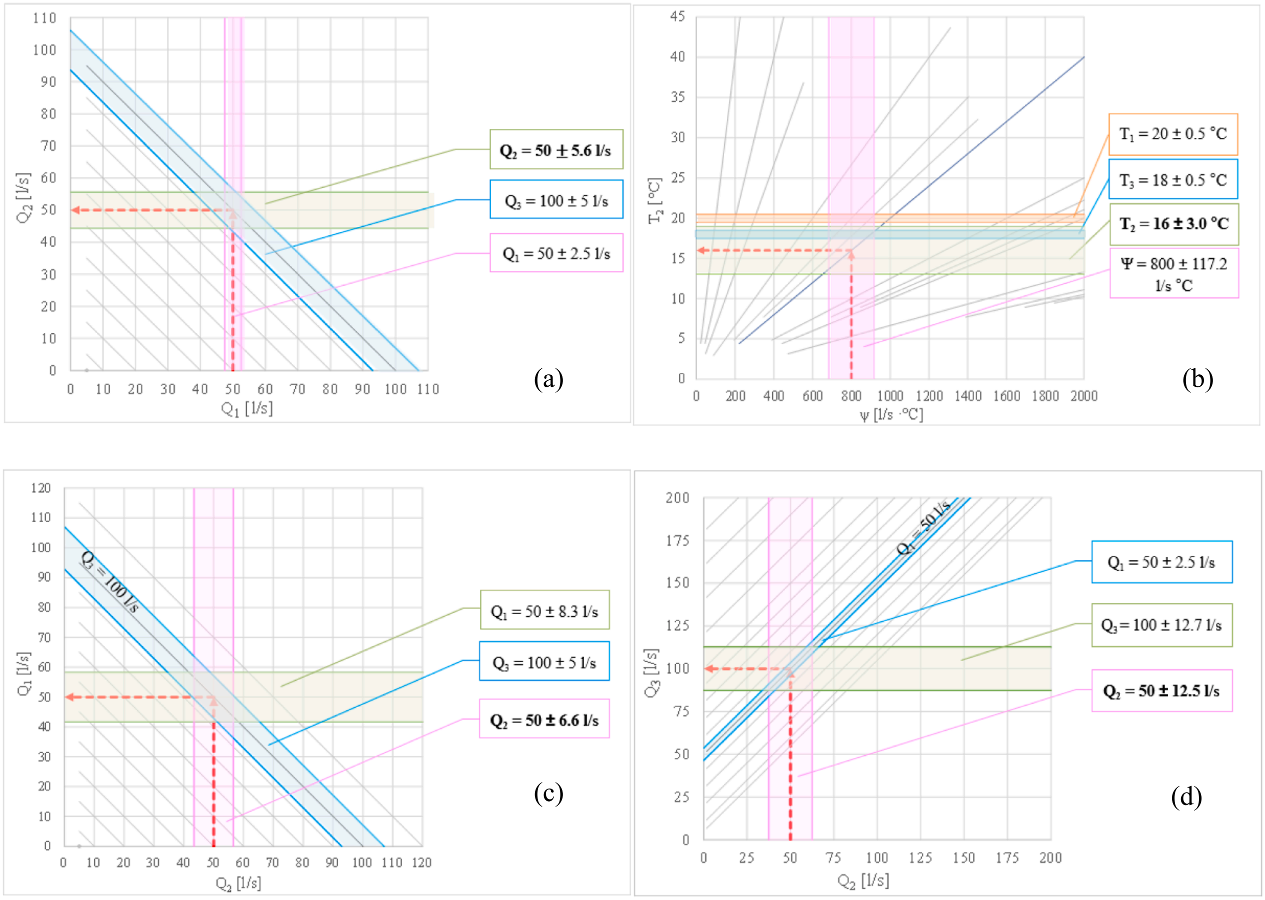

Fig. 2. Example 1. $U(Q_1) = U(Q_3) = 5$ %, $U(T_1) = U(T_3) = 0.5$ °C. (a) Estimation of Q_2, Scheme A. (b) Estimation of T_2, Scheme A; (c) Estimation of Q_2, Scheme B; (d) Estimation of Q_2, Scheme C.

Table 3
Resolution of the system of Eq. (1) for schemes A, B, and C, Example 2.

Scheme	Known variables				Unknown variables	
A	$Q_1 = 50$ l/s	$Q_3 = 60$ l/s	$T_1 =$ 20 °C	$T_3 =$ 18 °C	$Q_2 = 10$ l/s	$T_2 = 8$ °C
B	$Q_3 =$ 100 l/s	$T_1 =$ 23 °C	$T_2 =$ 30 °C	$T_3 =$ 25 °C	$Q_1 =$ 71.4 l/s	$Q_2 =$ 28.6 l/s
C	$Q_1 =$ 71.4 l/s	$T_1 =$ 23 °C	$T_2 =$ 30 °C	$T_3 =$ 25 °C	$Q_2 =$ 28.6 l/s	$Q_3 =$ 100 l/s

Table 4
Relative uncertainties of illicit flow rate and temperature, Example 2.

Scheme	Measurement uncertainties	$U(Q_2)/Q_2$	$U(T_2)/T_2$
A	$U(Q_i) = 5$ %, $U(T_j) = 0.5$ °C	39 %	111 %
	$U(Q_i) = 10$ %, $U(T_j) = 1.0$ °C	78 %	222 %
B	$U(Q_i) = 5$ %, $U(T_j) = 0.5$ °C	32 %	2 %
	$U(Q_i) = 10$ %, $U(T_j) = 1.0$ °C	64 %	3 %
C	$U(Q_i) = 5$ %, $U(T_j) = 0.5$ °C	44 %	2 %
	$U(Q_i) = 10$ %, $U(T_j) = 1.0$ °C	89 %	3 %

Particularly, the proposed procedure enables the selection of the most suitable configuration of flow probes and temperature sensors to get the best cost-effective solution and the highest reliability and accuracy of results. The study discusses three different schemes and performs the uncertainty analysis associated with each configuration according to the uncertainties due to the measuring equipment. The three schemes considered in the analysis include configurations of interest for practical applications in sewer networks. They consider as unknowable variables in the model the illicit flow and one of the two flow rates in the sewer (the upstream or downstream one) or its temperature.

Two case studies are presented and discussed. The first one consists of two meaningful computational examples for each of the three schemes mentioned above, respectively, considering the illicit flow quite similar or very different from the flow in the sewer pipe from the upstream section. The second is an application to an existing urban drainage system within the framework of the “PerFORM WATER 2030” project, funded by Regione Lombardia (Italy). The results confirm the goodness of the approach to detect and estimate illicit flows and its suitability as a support tool for planning field survey campaigns.

2. Material and methods

In the following analysis, a generic portion of the sewer network, with undefined length and diameter, is considered (Fig. 1); subscript 1 represents the upstream flow, subscript 3 the downstream flow, and subscript 2 the illicit flow(s) entering the system.

The variables of interest are six; the three temperatures T_1, T_2, and T_3, and the three flow rates Q_1, Q_2, and Q_3. Assuming steady conditions, when four quantities are measured then the system of Eq. (1) enables the calculation of the remaining two quantities:

$$\begin{cases} Q_1 + Q_2 = Q_3 \\ Q_1 \bullet T_1 + Q_2 \bullet T_2 = Q_3 \bullet T_3 \end{cases} \tag{1}$$

This study considers three different schemes of the field survey (Fig. A.0

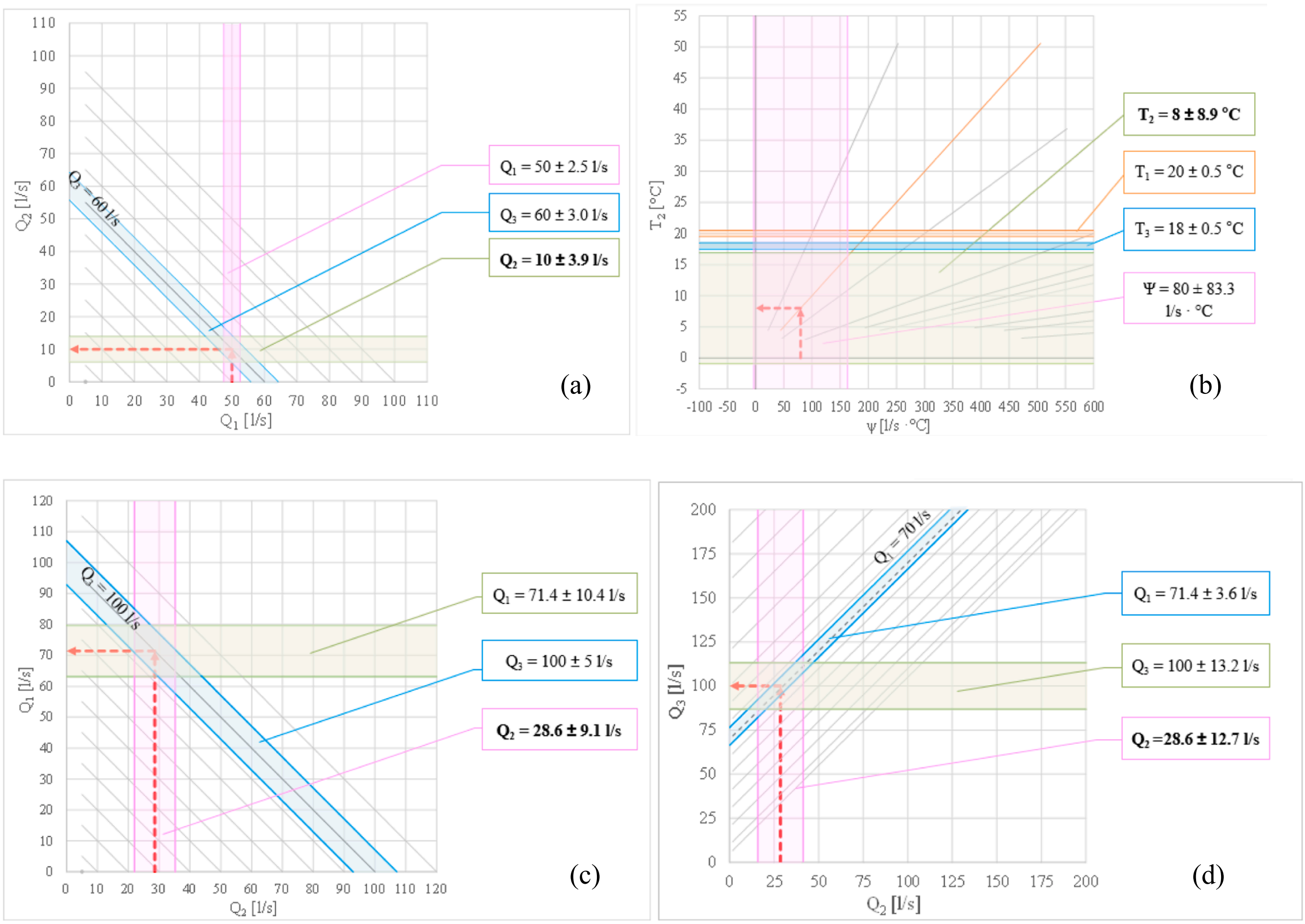

Fig. 3. Example 2. $U(Q_1) = U(Q_3) = 5$ %, $U(T_1) = U(T_3) = 0.5$ °C. (a) Estimation of Q_2, Scheme A; (b) Estimation of T_2, Scheme A; (c) Estimation of Q_2, Scheme B; (d) Estimation of Q_2, Scheme C.

in the Appendix section):

– A Scheme A: the unknown variables are Q2 and T2
– A Scheme B: the unknown variables are Q2 and Q1
– A Scheme C: the unknown variables are Q2 and Q3.

Schemes B and C require the knowledge of the temperature of the illicit source, while scheme A requires the knowledge of the stretch of the network affected by illicit flow(s). Scheme A corresponds to the typical case required to investigate groundwater infiltration. On the other hand, schemes B and C can be applied also with the DTS technique, which enables the measurement of the flow temperature along the cable (Beheshti and Saegrov, 2018; Schilperoort and Clemens, 2009). In practical applications, often, the kind of source is well-known by the operators (i.e., observing an increase in the amount of water discharged at the wastewater treatment plant in correspondence of the activation of the irrigation channel in the summer season), as well as the most critical stretches where, typically, floods occur.

The analysis hereby presented has assumed that all the flow meters and the temperature sensors have a fixed measurement uncertainty.

2.1. Scheme A

In this scheme, the flow rates, and the temperatures upstream and downstream are measured. The resolution of the system of Eq. (1) enables the calculation of the unknown variables Q_2 and T_2.

$$Q_2 = Q_3 - Q_1 \tag{2}$$

$$T_2 = \frac{Q_3 \bullet T_3 - Q_1 \bullet T_1}{Q_2} = \frac{\psi}{Q_2} \tag{3}$$

with $\psi = Q_3 \bullet T_3 - Q_1 \bullet T_1$. The dimensionless expression of Eq. (3) becomes:

$$\frac{T_2}{T_3} = \frac{Q_3}{Q_3 - Q_1} - \frac{Q_1}{Q_3 - Q_1} \bullet \frac{T_1}{T_3} \tag{4}$$

The relative uncertainty of the flow rate Q_2 has been calculated in terms of compound relative uncertainty (see the Appendix section for the detailed procedure). The obtained expressions have been rearranged to make them more usable from a practical point of view:

$$\frac{U(Q_2)}{Q_2} = \left[\frac{U(Q)}{Q}\right]_{1;3} \bullet \alpha \tag{5}$$

with $\alpha = \sqrt{2\text{Â}\cdot\left(\frac{Q_1}{Q_2}\right)^2 + 2\text{Â}\cdot\left(\frac{Q_1}{Q_2}\right) + 1}$. The parameter α has been introduced to make the expression more compact for practical purposes.

Being $\left[\frac{U(Q)}{Q}\right]_{1;3}$ the relative uncertainty of the measured flow rates (Q_1 and Q_3).

At the same way, the relative uncertainty of the estimated temperature T_2 is:

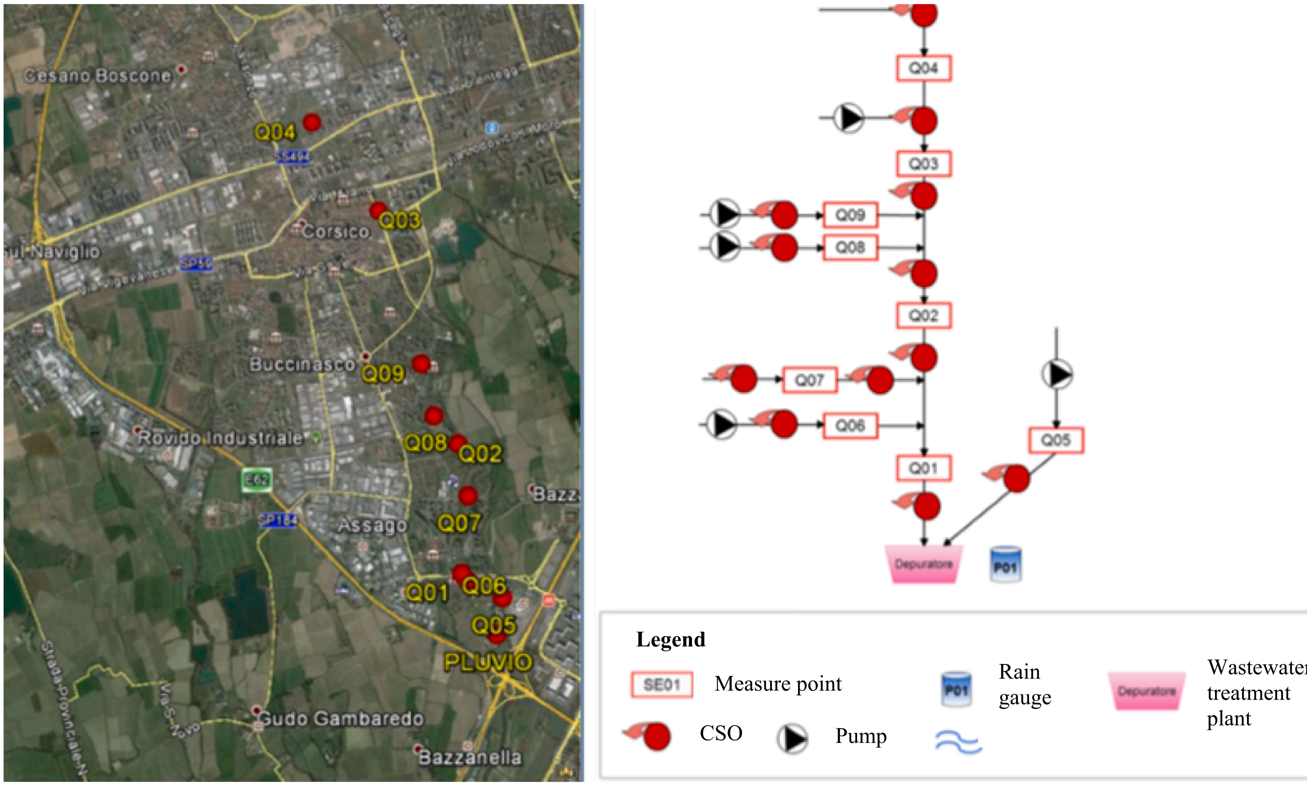

Fig. 4. Map and schematization of the sewer network discharging to the Assago wastewater treatment plant.

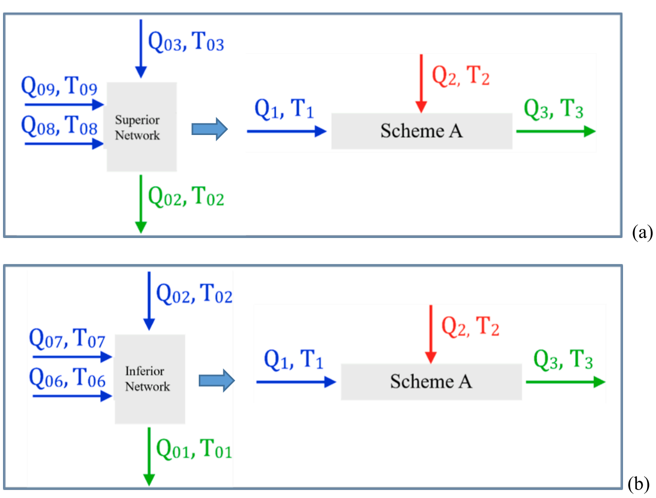

Fig. 5. Relation between the Superior (a) and Inferior (b) Network to the benchmark Scheme A.

$$\frac{U(T_2)}{T_2}=\sqrt{\left[\frac{U(Q)}{Q}\right]^2_{1;3}\bullet\left(\frac{(T_1\bullet Q_1)^2+(T_3\bullet Q_3)^2}{(Q_2\bullet T_2)^2}+\alpha^2\right)+\left[U^2(T)\right]_{1;3}\bullet\frac{1}{T_2^2}\bullet\alpha^2} \quad (6)$$

being $\left[U^2(T)\right]_{1;3}$ the uncertainty of the measured temperatures (T_1 and T_3).

2.2. Scheme B

This scheme assumes that all the temperatures and the downstream flow rates are measured. Again, the resolution of the system of Eq. (1) enables the calculation of the two unknown variables, Q_1 and Q_2.

$$Q_2 = Q_3\bullet\frac{\Delta T_{31}}{\Delta T_{21}} \quad (7)$$

with $\Delta T_{31} = T_3 - T_1$ and $\Delta T_{21} = T_2 - T_1$. So:

$$Q_1 = Q_3 - Q_2 = Q_3\bullet\left(1-\frac{\Delta T_{31}}{\Delta T_{21}}\right) \quad (8)$$

The dimensionless forms of the Eqs. (7) and (8) are, respectively:

$$\frac{Q_1}{Q_3} = 1-\frac{\Delta T_{31}}{\Delta T_{21}} = \frac{\Delta T_{23}}{\Delta T_{21}} \quad (9)$$

$$\frac{Q_2}{Q_3} = \frac{\Delta T_{31}}{\Delta T_{21}} \quad (10)$$

The relative uncertainties of the estimated flow rates Q_2 and Q_1 have been calculated in terms of compound relative uncertainty (see the Appendix section for the detailed procedure). The obtained expressions have been rearranged to make them more usable from a practical point of view:

$$\frac{U(Q_2)}{Q_2} = \sqrt{\left[\frac{U(Q)}{Q}\right]^2_3 + \left[U^2(T)\right]_{1;2;3}\bullet\beta} \quad (11)$$

$$\frac{U(Q_1)}{Q_1} = \sqrt{\left[\frac{U(Q)}{Q}\right]^2_3\bullet\left(\left(\frac{Q_2}{Q_1}\right)^2+\left(\frac{Q_3}{Q_1}\right)^2\right)+\left(\frac{Q_2}{Q_1}\right)^2\bullet\left[U^2(T)\right]_{1;2;3}\bullet\beta} \quad (12)$$

with $\beta = \frac{1}{\Delta T_{31}{}^2}\bullet\left(1+\left(\frac{\Delta T_{32}}{\Delta T_{21}}\right)^2+\left(\frac{\Delta T_{31}}{\Delta T_{21}}\right)^2\right)$ and $\Delta T_{32} = T_3 - T_2$.

being $\left[U^2(T)\right]_{1;2;3}$ the uncertainty of the measured temperatures, while $\left[\frac{U(Q)}{Q}\right]_3$ is the relative uncertainty of the measured flow rate Q_3.

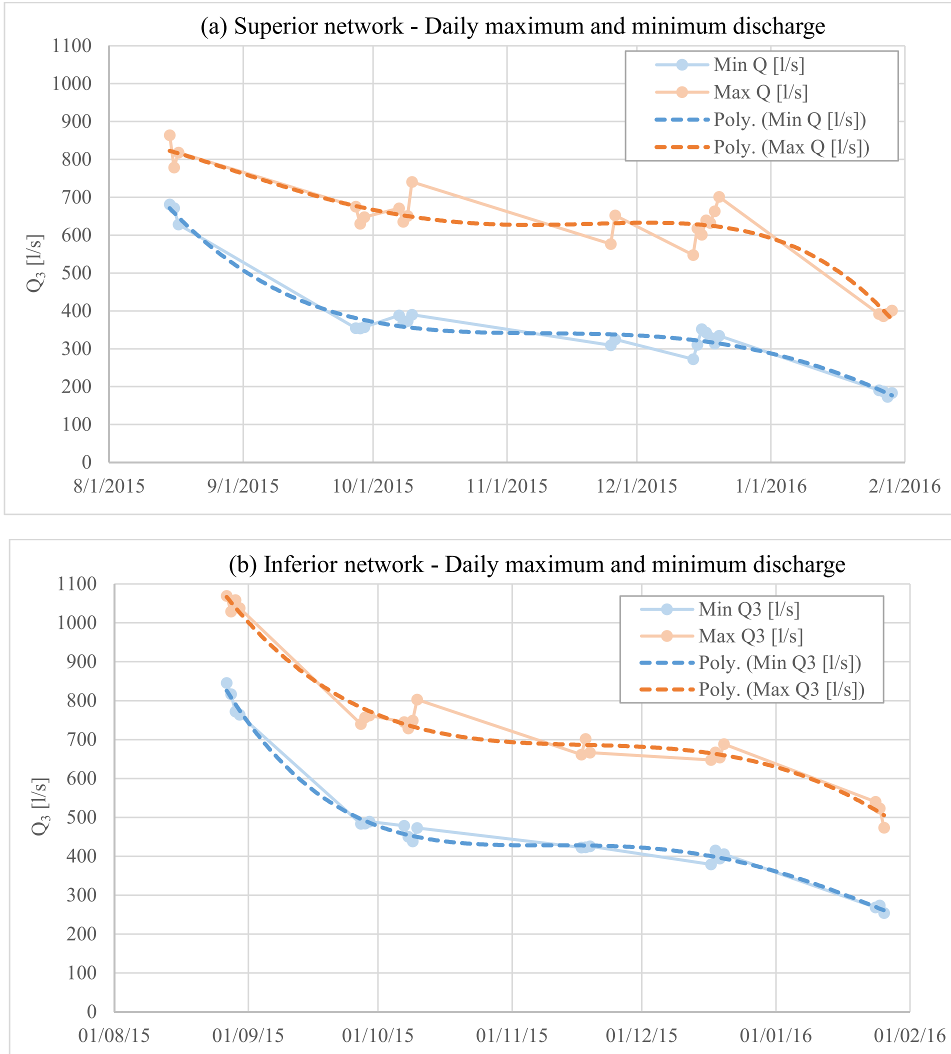

Fig. 6. Daily maximum and minimum discharge at the downstream node for both the Superior (a) and Inferior (b) networks.

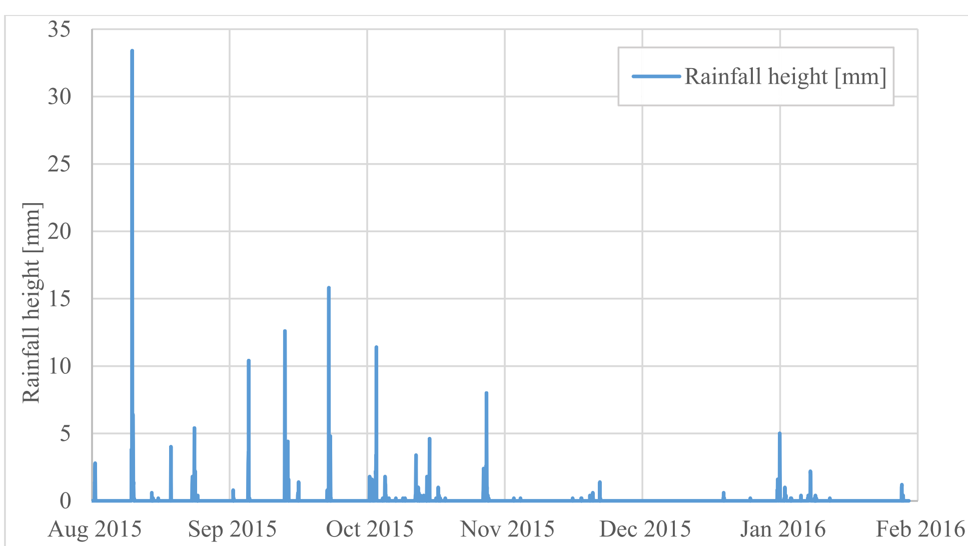

Fig. 7. Rainfall depth in the recorded period.

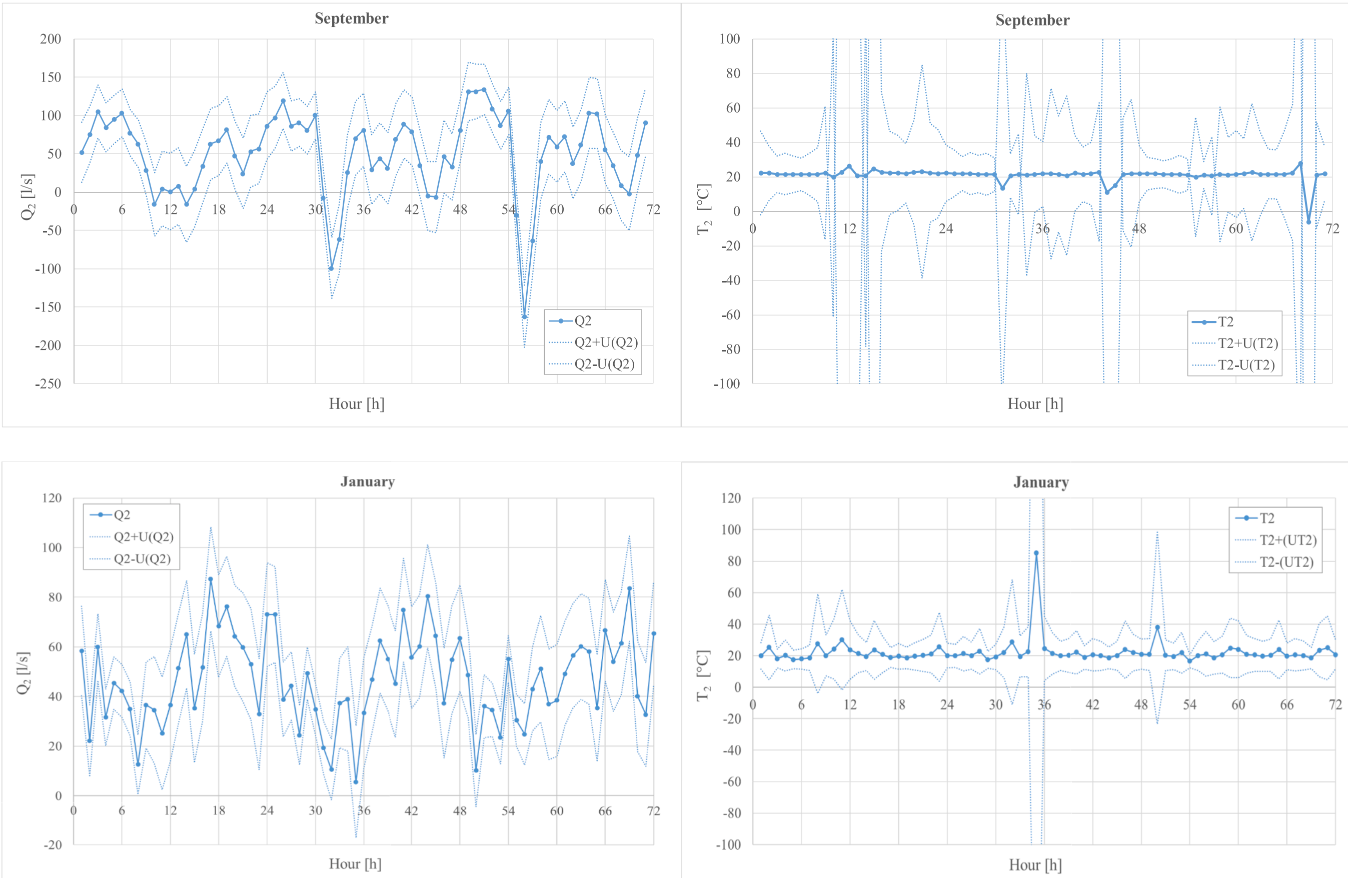

Fig. 8. Estimation of the flow rate and temperature of illicit flows and their range of uncertainty for both the Superior (a and b) and Inferior (c and d) network for September and January survey data.

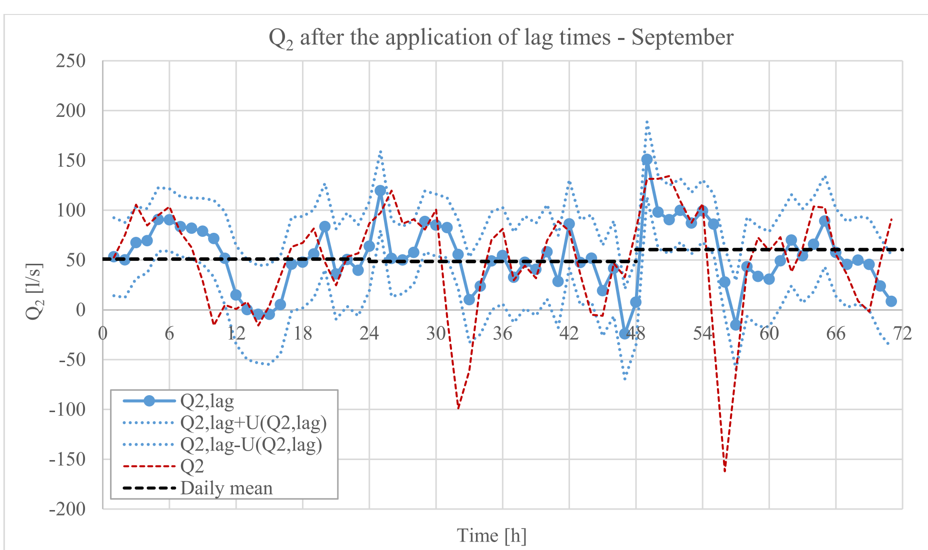

Fig. 9. Application of lag time for the estimation of Q_2.

2.3. Scheme C

This scheme assumes that all the temperatures and the upstream flow rate are measured. Once more, the resolution of the system of Eq. (1) enables the estimation of the unknown variables Q_2 and Q_3.

$$Q_2 = Q_1 \bullet \frac{\Delta T_{31}}{\Delta T_{23}} \tag{13}$$

$$Q_3 = Q_1 + Q_2 = Q_1 \bullet \left(1 + \frac{\Delta T_{31}}{\Delta T_{23}}\right) \tag{14}$$

with $\Delta T_{23}= T_2 - T_3$. The dimensionless form of Eqs. (13) and (14) are:

$$\frac{Q_3}{Q_1} = 1 + \frac{\Delta T_{31}}{\Delta T_{23}} = \frac{\Delta T_{21}}{\Delta T_{23}} \tag{15}$$

$$\frac{Q_2}{Q_1} = \frac{\Delta T_{31}}{\Delta T_{23}} \tag{16}$$

The relative uncertainties of the estimated flow rates Q_3 and Q_2 have been estimated in terms of compound relative uncertainty (see the Appendix section for the detailed procedure). The obtained expressions have been rearranged to make them more usable from a practical point of view:

$$\frac{U(Q_3)}{Q_3} = \sqrt{\left[\frac{U(Q)}{Q}\right]_1^2 \bullet \left(\left(\frac{Q_1}{Q_3}\right)^2 + \left(\frac{Q_2}{Q_3}\right)^2\right) + \left(\frac{Q_2}{Q_3}\right)^2 \bullet \left[U^2(T)\right]_{1;2;3} \bullet \gamma} \tag{17}$$

$$\frac{U(Q_2)}{Q_2} = \sqrt{\left[\frac{U(Q)}{Q}\right]_1^2 + \left[U^2(T)\right]_{1;2;3} \bullet \gamma} \tag{18}$$

with $\gamma = \left(\frac{1 + \left(\frac{\Delta T_{31}}{\Delta T_{23}}\right)^2 + \left(\frac{\Delta T_{21}}{\Delta T_{23}}\right)^2}{\Delta T_{31}{}^2}\right)$, while $\left[\frac{U(Q)}{Q}\right]_1$ is the relative uncertainty of the measured flow rate Q_1.

2.4. Remarks

In unsteady conditions the analysis should keep into account a lag time to make coherent the measures in the upstream flow with the ones collected in the downstream section. In this paper, the lag time has been estimated for each trunk through quantitative and qualitative methods: in the first approach, dividing the distance from the closing section by an average velocity, which has been assumed equal to 0.5 m/s; in the second approach, considering the delay between the upstream and downstream hydrographs. To use a single set of lag times and average them to identify a constant value is a simplified hypothesis.

In addition to that, in both steady conditions and unsteady conditions, the temperature in the mainstream could be altered just because of the heat exchange between with the air above and the streambed around.

Moreover, it could happen that there are some unmonitored but licit inflows in the investigated stretch of the system.

The imperfect knowledge about the system topology could be taken into account by considering additional uncertainty in the estimation of the unknown variable.

3. Computational application

The graphical results of the application of Eqs. (2), (3), (4), (7), (8), (9), (10), (13), (15) and (16) have been represented, in Figs. A.1–A.11 of the Appendix section. The following computational applications aim to investigate the reliability and accuracy of the three schemes in estimating illicit flows. In the examples, all the flow meters have the same relative uncertainty (expressed as %), and all the temperature sensors have the same absolute uncertainty (expressed as °C). Two values for each variable, $U(Q_i) = 5$–10 %, and $U(T_i) = 0.5$–1.0 °C, are considered. Example 1 serves as a benchmark, as the upstream flow rate Q_1 and illicit flow rate Q_2 are assumed to be equal (Fig. A.12 in the Appendix section). On the contrary, Example 2 represents an extreme situation when Q_2 is significantly smaller than Q_1 (Fig. A.13 in the Appendix section).

3.1. Example 1

The two unknown variables are calculated by Eqs. (2) and (3) for Scheme A, Eqs. (7), and (8) for Scheme B, and Eqs. (13) and (14) for Scheme C (Table 1).

Then, focusing on the illicit flow, Eqs. (5) and (6) enable the estimation of the relative uncertainties $U(Q_2)/Q_2$ and $U(T_2)/T_2$ for each of the three schemes (Table 2).

According to Eqs. (5), (6), (11), and (18), doubling the uncertainty of both the measured flow rates $U(Q_i)$ and of the temperatures $U(T_i)$, the relative uncertainty of the estimation of the illicit flow rate $U(Q_2)/Q_2$ and of the temperature $U(T_2)/T_2$ doubles as well. The minimum relative uncertainty for illicit flow rate estimation $U(Q_2)/Q_2$ occurs in Scheme A, since the unknown flow rate Q_2 is calculated directly from the balance equation. Differently, for schemes B and C, the flow rate Q_2 is estimated by the system of Eq. (1). Comparing flow rate uncertainties, Scheme B provides a more accurate estimation than Scheme C; this highlights the importance of this kind of analysis when deciding the setup of the survey instruments. But, as a matter of fact, flow meters are generally more expensive than temperature sensors; for this reason, schemes B and C can be significantly more money-saving than schemes A. Concerning the relative uncertainty for illicit flow temperature $U(T_2)/T_2$, it presents the highest value in Scheme A, where it is not measured directly in the field but estimated on the basis of the combination of other uncertainties. The relative uncertainty of the illicit flow temperature is minimum for Scheme B and Scheme C since, in this case, the temperature T_2 is measured.

In conclusions, Scheme B can offer a compromise between costs and benefits, because it requires a less expensive setup than Scheme A and has a better efficiency than Scheme C. Fig. 2a-2b-2c-2d shows, graphically, the range of illicit flow rates and temperatures (if unknown) for schemes A, B, and C, assuming an uncertainty $U(Q_i) = 5$ % for the measured flow rates and $U(T_i) = 0.5$ °C for the measured temperatures.

3.2. Example 2

The two unknown variables are calculated by Eqs. (2) and (3) for Scheme A, Eqs. (7), and (8) for Scheme B, and Eqs. (13) and (14) for Scheme C (Table 3).

Then, focusing on the illicit flow, Eqs. (5) and (6), enable the estimation of the relative uncertainties $U(Q_2)/Q_2$ and $U(T_2)/T_2$ for each one of the three schemes (Table 4).

Scheme B proves to be the most suitable, having the lowest relative uncertainty of illicit flow rate and temperature. The unbalance between Q_1 and Q_2 in Example 2 involves a high uncertainty in the estimation of T_2 for Scheme A. It implies a difficult identification of the illicit flow source. As discussed in Example 1, doubling the uncertainty of both the measured flow rates $U(Q_i)$ and of the temperatures $U(T_i)$, the relative uncertainty in the estimation of illicit flow rate $U(Q_2)/Q_2$ and temperature $U(T_2)/T_2$ doubles, as well. Fig. 3a-3b-3c-3d show graphically the flow rate and temperature values of illicit flow and their uncertainties for schemes A, B, and C, assuming a relative uncertainty of measured flow rate $U(Q_i) = 5$ % and temperature $U(T_i) = 0.5$ °C.

It must be remarked that the relative uncertainties result to be higher in Example 2 than in Example 1. This means that when the flow rates of illicit flow Q_2 and upstream flow Q_1 are similar, the uncertainties of the estimated variables are lower than in the case in which Q_2 is much smaller than Q_1.

4. Case study

This framework has been tested also on the downstream branches of the combined sewer network conveying waste waters and storm waters to the wastewater treatment plant of Assago (Milano, Italy). This portion of the urban sewer network is suspected to be affected by illicit flows, especially infiltrations caused by channels and ditches used for irrigation during spring and summer, increasing the groundwater level. Data from the field campaign, carried out from September 2015 to January 2016, provided to the Authors by the Integrated Water Service multiutility CAP Holding S.p.A., have been used in the analysis. The measurements have been performed by means of area-velocity flow meters with one minute time resolution, together with temperature sensors (Figs. A.14-A.17 in the Appendix section). Rainfall data used in the analysis have been recorded at the pluviographic station of the Assago wastewater treatment plant. Fig. 4 shows the map and the scheme of the drainage system. The nine measurement points in the main branches have been labelled as Q0#, being # = 1, …, 9.

The selected portions of the sewer network can be seen as subdivided into two parts: a Superior Network, including nodes 2, 3, 8, and 9, and an Inferior Network, including nodes 1, 2, 6, and 7. They can be related to Scheme A assuming $Q_1 = Q_{03} + Q_{08} + Q_{09}$, $Q_3 = Q_{02}$, $T_1 = (Q_{03} \cdot T_{03} + Q_{09} \cdot T_{09} + Q_{08} \cdot T_{08})/(Q_{03} + Q_{08} + Q_{09})$, and $T_3 = T_{02}$ for the Superior Network (Fig. 5a), and $Q_1 = Q_{02} + Q_{06} + Q_{07}$, $Q_3 = Q_{01}$, $T_1 = (Q_{02} \cdot T_{02} + Q_{06} \cdot T_{06} + Q_{07} \cdot T_{07})/(Q_{02} + Q_{06} + Q_{07})$, $T_3 = T_{01}$ for the Inferior Network (Fig. 5b).

As shown in Fig. 6a and Fig. 6b (about respectively the Superior and Inferior Network), the minimum flow rate measured at the downstream node (typically occurring at night) decreases from September to January. It can be associated with the closure of the channels at the end of the irrigation period with the consequent decrease of infiltrations into the sewer system. During the summer, they are used regularly for irrigation purposes, and so they have a significant water level; since they transport a lot of water, a portion of it percolates (due to the imperfect sealing of the stream bed) into the water table, increasing its level. With a higher level of the water table, the groundwater infiltration increases. In autumn, the channels are less used, while during the winter they are closed and, so, the water table level lowers (also because of the lower precipitations), explaining the low discharges recorded in January.

The trend is also strengthened by the decrease in rainfall events and volume in winter (Fig. 7).

The flow rate and the temperature of illicit flows and their range of uncertainty have been estimated by means of Eqs. (2), (3), (5), and (6) for the recorded period. Fig. 8a-b-c-d show the results for respectively the first and the last months of the analysis (September and January).

As already discussed about the computational examples, when the flow rate of illicit flow is significantly lower than the upstream flow, the uncertainty in estimating the temperature T_2 increases for Scheme A. The negative values of the flow rate need a deeper investigation. In fact, since there are no pumping stations in the area, they could indicate exfiltration from the sewer network when a high filling occurs. To verify this assumption, the water level inside the pipes of the sewer has been estimated. The results have shown that whenever the water level rises then Q_2 experiences a negative value. In addition, as already stated about unsteady conditions, the analysis should keep into account a lag time to make coherent the measures in the upstream section with the ones collected in the downstream section. This lag time has been estimated for each trunk through both quantitative and qualitative methods: in the first approach, dividing the distance from the closing section by an average velocity, which has been assumed equal to 0.5 m/s; in the second approach, estimating the delay between the upstream and downstream hydrographs. To use a single set of lag times and average them to identify a constant value is a simplified hypothesis. However, its application has allowed good results in reducing the negative values of illicit flow rate Q_2, as shown in Fig. 9 from the comparison between Q_2 (illicit flow without considering the time lag) and $Q_{2,lag}$ (illicit flow corrected by applying the time lag).

5. Conclusions

The potential of integrating punctual flow rate and temperature measurements to estimate illicit flows in sewer networks has been investigated. The aim is to identify the best configuration of flow meters and temperature sensors, under different conditions, to maximize reliability, accuracy, and cost-effectiveness. To do this, the uncertainty in the estimations, derived from those of the instruments, has been considered. Three typical schemes of practical interest have been compared by means of some meaningful computational examples. A general result, largely expected, is that when the illicit and the sewer flow rates are very different, the reliability and accuracy of the model prediction decreases. When applicable, the scheme with three temperature sensors and a single flow meter seems the most convenient in terms of both costs and reliability. When the suspected point of inflow is not accessible, positioning the flow meter in the upstream section instead of the downstream one decreases the uncertainty on the estimated values of the unknown variables (the illicit and the downstream flow rates). In general, temperature measurement techniques work well if the temperature of illicit flow is not very similar to those of the flow rate in the system. The application to a case study near to Milano (Italy), in the framework of the research project PerFORM WATER 2030, has confirmed the goodness of the proposed procedure to estimate illicit flows. Results have clearly shown that the portion of the sewer investigated is dangerously affected by illicit flows, as then verified by the use of the DTS technique. In unsteady conditions, the estimations must keep into account the lag time delaying the measures upstream and downstream the considered trunk. In addition to that, in both steady conditions and unsteady conditions, the temperature in the mainstream could be altered just because of the heat exchange between with the air above and the streambed around. To investigate this effect, further development of the study will include a heat transport and exchange model. The simplified estimation of the lag time used in this paper looks anyway an adequate tool to be used in preliminary analysis, to plan more accurate field surveys.

CRediT authorship contribution statement

Anita Raimondi: Writing – review & editing, Writing – original draft, Validation, Supervision, Methodology, Investigation, Formal analysis, Data curation, Conceptualization. **Umberto Sanfilippo:** Writing – review & editing, Validation, Supervision, Methodology, Investigation, Formal analysis, Data curation, Conceptualization. **Gianfranco Becciu:** Project administration, Funding acquisition.

Declaration of competing interest

The authors declare that they have no known competing financial interests or personal relationships that could have appeared to influence the work reported in this paper.

Data availability

Data will be made available on request.

Acknowledgments

The Authors wish to thank CAP Holding S.p.A. for sharing the field survey data of the sewage network discharging to the Assago wastewater treatment plant.

Fundings

This research has been funded by Regione Lombardia, within the framework of the project “PerFORM WATER 2030”.

Appendix

Procedure to estimate the compound relative uncertainty.

General expressions:

$$w = w(x_1,\ x_2,\ \dots,\ x_i,\ \dots,\ x_N)$$

$$s_w{}^2 = \left(\frac{\partial w}{\partial x_1}\right)^2 \cdot s_{x_1}{}^2 + \left(\frac{\partial w}{\partial x_2}\right)^2 \cdot s_{x_2}{}^2 + \dots + \left(\frac{\partial w}{\partial x_i}\right)^2 \cdot s_{x_i}{}^2 + \dots + \left(\frac{\partial w}{\partial x_N}\right)^2 \cdot s_{x_N}{}^2$$

s_w: expected uncertainty of a generic variable w that is function of one or more independent variables x_i that are also affected by a certain variability $[s_{x_1}, s_{x_1}, \cdots, s_{x_i}, \cdots, s_{x_N}]$.

Application to the three schemes of reference:

Scheme A

$$U(Q_2) = \sqrt{U^2(Q_1) + U^2(Q_3)} \tag{19}$$

$$U(T_2) = \frac{1}{Q_2} \bullet \sqrt{T_1{}^2 \bullet U^2(Q_1) + T_3{}^2 \bullet U^2(Q_3) + Q_1{}^2 \bullet U^2(T_1) + Q_3{}^2 \bullet U^2(T_3) + T_2{}^2 \bullet U^2(Q_2)} \tag{20}$$

Equation (20) can be rewritten substituting the uncertainty $U^2(Q_2)$ with Eq. (19); so, a simpler form without any implicit term is found and only measured quantities enter the equation:

$$U(T_2) = \frac{1}{Q_2} \bullet \sqrt{U^2(Q_1) \bullet \left(T_1{}^2 + T_2{}^2\right) + U^2(Q_3) \bullet \left(T_3{}^2 + T_2{}^2\right) + Q_1{}^2 \bullet U^2(T_1) + Q_3{}^2 \bullet U^2(T_3)} \tag{21}$$

To make the equations more usable in practice they have been rearranged as follows:

$$\frac{U(Q_2)}{Q_2} = \frac{1}{Q_2} \bullet \left[\frac{U(Q)}{Q}\right]_{1;3} \bullet \sqrt{Q_1{}^2 + Q_3{}^2} = \left[\frac{U(Q)}{Q}\right]_{1;3} \bullet \sqrt{\left(\frac{Q_1}{Q_2}\right)^2 + \left(\frac{Q_3}{Q_2}\right)^2} = \left[\frac{U(Q)}{Q}\right]_{1;3} \bullet \alpha \tag{22}$$

$$\begin{aligned}
\frac{U(T_2)}{T_2} &= \frac{1}{Q_2 \bullet T_2} \bullet \sqrt{\left[\frac{U(Q)}{Q}\right]^2_{1;3} \bullet \left(T_1{}^2 \bullet Q_1{}^2 + T_3{}^2 \bullet Q_3{}^2\right) + \left[U^2(T)\right]_{1;3} \bullet \left(Q_1{}^2 + Q_3{}^2\right) + T_2{}^2 \bullet Q_2{}^2 \bullet \left(\frac{U(Q_2)}{Q_2}\right)^2} \\
&= \sqrt{\left[\frac{U(Q)}{Q}\right]^2_{1;3} \bullet \frac{\left(T_1{}^2 \bullet Q_1{}^2 + T_3{}^2 \bullet Q_3{}^2\right)}{(Q_2 \bullet T_2)^2} + \left[U^2(T)\right]_{1;3} \bullet \frac{\left(Q_1{}^2 + Q_3{}^2\right)}{(Q_2 \bullet T_2)^2} + \left[\frac{U(Q)}{Q}\right]^2_{1;3} \bullet \left(\frac{Q_1}{Q_2}\right)^2 + \left(\frac{Q_3}{Q_2}\right)^2} \\
&= \sqrt{\left[\frac{U(Q)}{Q}\right]^2_{1;3} \bullet \left(\frac{\left(T_1{}^2 \bullet Q_1{}^2 + T_3{}^2 \bullet Q_3{}^2\right)}{(Q_2 \bullet T_2)^2} + \left(\frac{Q_1}{Q_2}\right)^2 + \left(\frac{Q_3}{Q_2}\right)^2\right) + \left[U^2(T)\right]_{1;3} \bullet \frac{\left(Q_1{}^2 + Q_3{}^2\right)}{(Q_2 \bullet T_2)^2}} \\
&= \sqrt{\left[\frac{U(Q)}{Q}\right]^2_{1;3} \bullet \left(\frac{(T_1 \bullet Q_1)^2 + (T_3 \bullet Q_3)^2}{(Q_2 \bullet T_2)^2} + \alpha^2\right) + \left[U^2(T)\right]_{1;3} \bullet \frac{1}{T_2{}^2} \bullet \alpha^2}
\end{aligned} \tag{23}$$

Scheme B

$$U(Q_1) = \sqrt{U^2(Q_2) + U^2(Q_3)} \tag{24}$$

$$\begin{aligned}
U(Q_2) &= \frac{1}{|\Delta T_{21}|} \bullet \sqrt{\Delta T_{31}{}^2 \bullet U^2(Q_3) + Q_3{}^2 \bullet U^2(T_3) + Q_3{}^2 \bullet \left(\frac{\Delta T_{32}}{\Delta T_{21}}\right)^2 \bullet U^2(T_1) + Q_3{}^2 \bullet \left(\frac{\Delta T_{31}}{\Delta T_{21}}\right)^2 \bullet U^2(T_2)} = \\
&= \frac{Q_3}{|\Delta T_{21}|} \bullet \sqrt{\Delta T_{31}{}^2 \bullet \left[\frac{U(Q)}{Q}\right]^2_{3} + \left[U^2(T)\right]_{1;2;3} \bullet \left(1 + \left(\frac{\Delta T_{32}}{\Delta T_{21}}\right)^2 + \left(\frac{\Delta T_{31}}{\Delta T_{21}}\right)^2\right)}
\end{aligned} \tag{25}$$

Equation (24) can be rewritten substituting the uncertainty $U^2(Q_2)$ with Eq. (25); so, an expression without any implicit term is found, with only measured quantities. To make the equations more usable in practice they have been rearranged as follows:

$$\frac{U(Q_1)}{Q_1} = \frac{1}{Q_1} \bullet \sqrt{Q_2{}^2 \bullet \left(\frac{U(Q_2)}{Q_2}\right)^2 + Q_3{}^2 \bullet \left[\frac{U(Q)}{Q}\right]_3^2} = \sqrt{\left(\frac{Q_2}{Q_1}\right)^2 \bullet \left(\frac{U(Q_2)}{Q_2}\right)^2 + \left(\frac{Q_3}{Q_1}\right)^2 \bullet \left[\frac{U(Q)}{Q}\right]_3^2} = \sqrt{\left[\frac{U(Q)}{Q}\right]_3^2 \bullet \left(\left(\frac{Q_2}{Q_1}\right)^2 + \left(\frac{Q_3}{Q_1}\right)^2\right) + \left(\frac{Q_2}{Q_1}\right)^2 \bullet \left[U^2(T)\right]_{1;2;3} \bullet \beta} \tag{26}$$

$$\frac{U(Q_2)}{Q_2} = \frac{Q_3}{Q_2} \bullet \frac{1}{|\Delta T_{21}|} \bullet \sqrt{\Delta T_{31}{}^2 \bullet \left[\frac{U(Q)}{Q}\right]_3^2 + \left[U^2(T)\right]_{1;2;3} \bullet \left(1 + \left(\frac{\Delta T_{32}}{\Delta T_{21}}\right)^2 + \left(\frac{\Delta T_{31}}{\Delta T_{21}}\right)^2\right)} = \sqrt{\left[\frac{U(Q)}{Q}\right]_3^2 + \left[U^2(T)\right]_{1;2;3} \bullet \frac{\left(1 + \left(\frac{\Delta T_{32}}{\Delta T_{21}}\right)^2 + \left(\frac{\Delta T_{31}}{\Delta T_{21}}\right)^2\right)}{\Delta T_{31}{}^2}} = \sqrt{\left[\frac{U(Q)}{Q}\right]_3^2 + \left[U^2(T)\right]_{1;2;3} \bullet \beta} \tag{27}$$

Scheme C

$$U(Q_2) = \frac{Q_1}{|\Delta T_{23}|} \bullet \sqrt{\Delta T_{31}{}^2 \bullet \left[\frac{U(Q)}{Q}\right]_1^2 + \left[U^2(T)\right]_{1;2;3} \bullet \left(1 + \left(\frac{\Delta T_{31}}{\Delta T_{23}}\right)^2 + \left(\frac{\Delta T_{21}}{\Delta T_{23}}\right)^2\right)} \tag{28}$$

$$U(Q_3) = \frac{Q_1}{|\Delta T_{23}|} \bullet \sqrt{\left[\frac{U(Q)}{Q}\right]_1^2 \bullet \left(\Delta T_{31}{}^2 + \Delta T_{23}{}^2\right) + \left[U^2(T)\right]_{1;2;3} \bullet \left(1 + \left(\frac{\Delta T_{31}}{\Delta T_{23}}\right)^2 + \left(\frac{\Delta T_{21}}{\Delta T_{23}}\right)^2\right)} \tag{29}$$

To make the equations more usable in practice, they have been rearranged as follows:

$$\frac{U(Q_2)}{Q_2} = \sqrt{\left[\frac{U(Q)}{Q}\right]_1^2 + \left[U^2(T)\right]_{1;2;3} \bullet \gamma} \tag{30}$$

$$\frac{U(Q_3)}{Q_3} = \sqrt{\left[\frac{U(Q)}{Q}\right]_1^2 \bullet \left(\left(\frac{Q_1}{Q_3}\right)^2 + \left(\frac{Q_2}{Q_3}\right)^2\right) + \left(\frac{Q_2}{Q_3}\right)^2 \bullet \left[U^2(T)\right]_{1;2;3} \bullet \gamma} \tag{31}$$

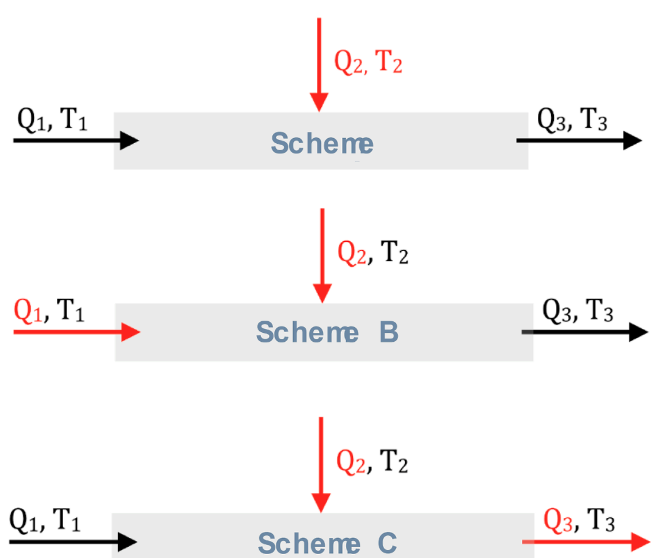

Fig. A.0. Schemes of reference.

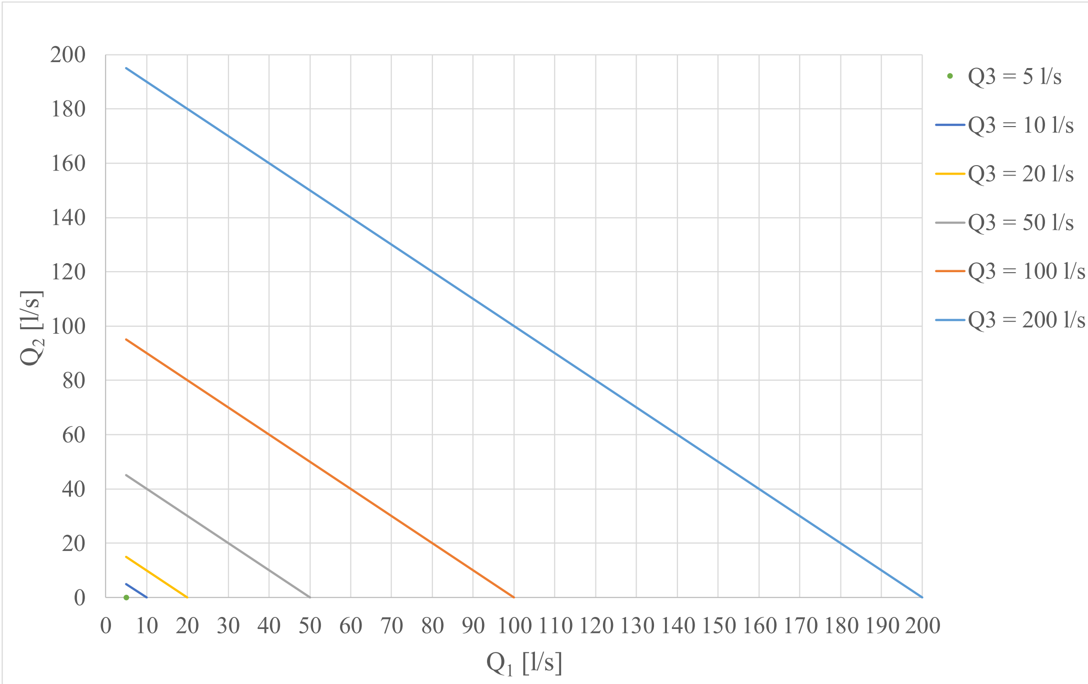

Fig. A.1. Estimation of Q_2, Scheme A (Eq. (2)).

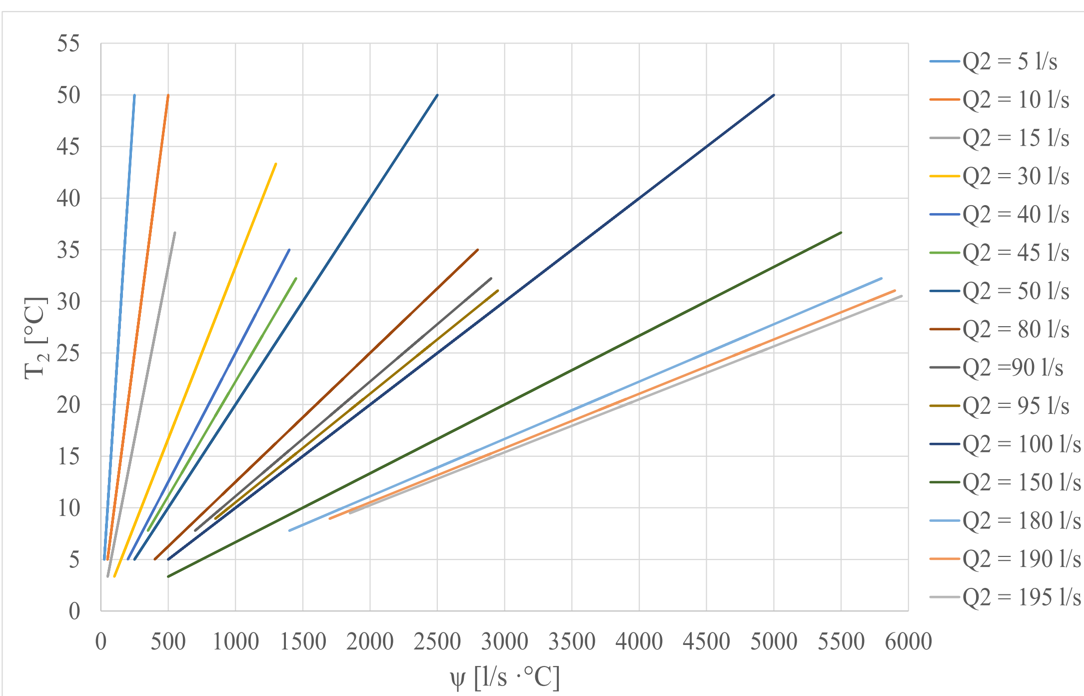

Fig. A.2. Estimation of T_2, Scheme A (Eq. (3)).

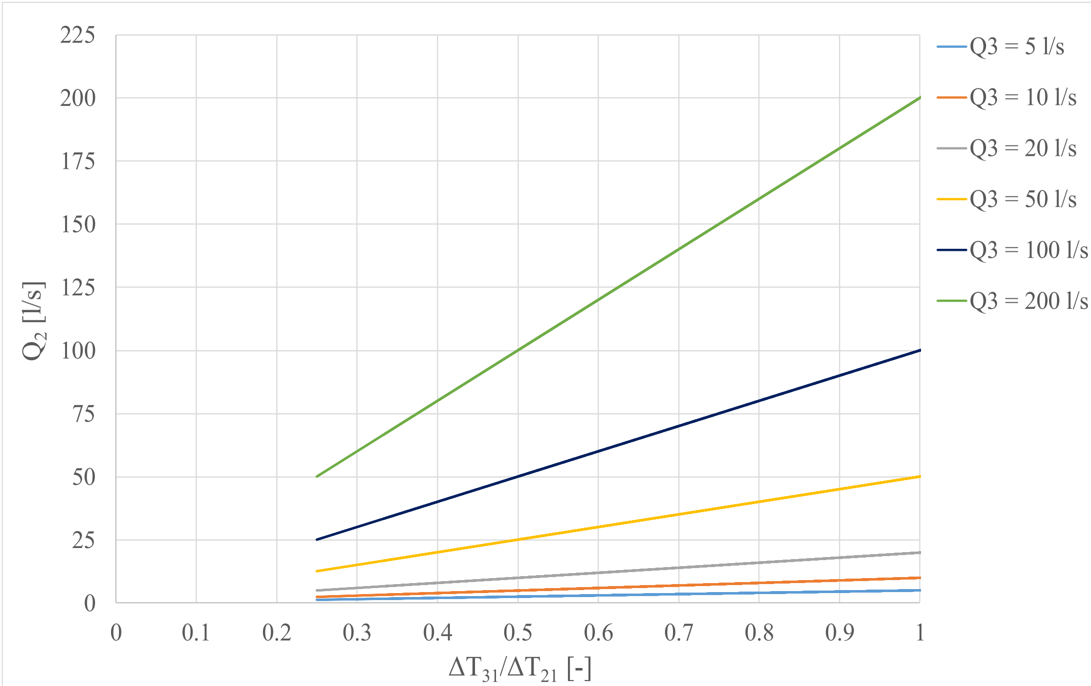

Fig. A.3. Estimation of Q_2, Scheme B (Eq. (7)).

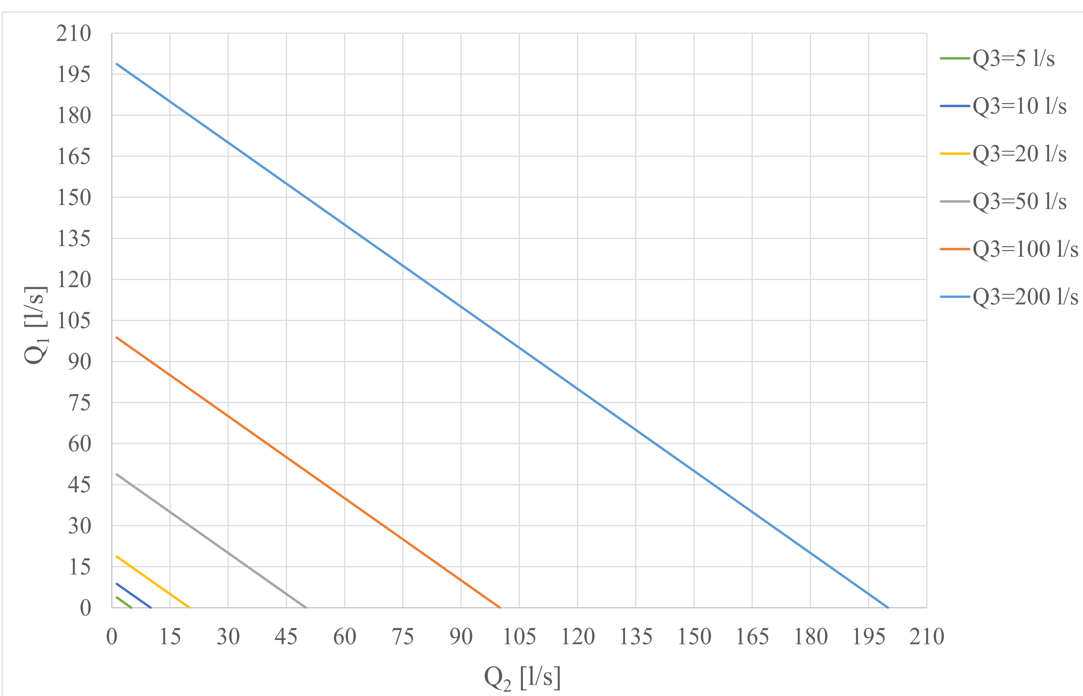

Fig. A.4. Estimation of Q_1, Scheme B (Eq. (8)).

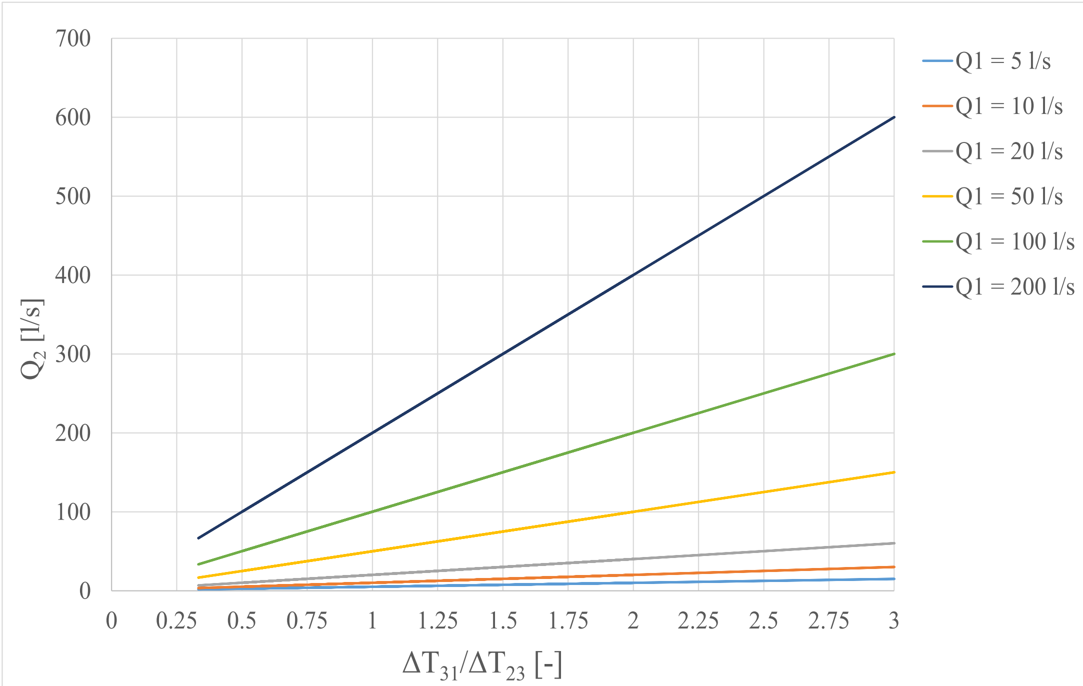

Fig. A.5. Estimation of Q_2, Scheme C (Eq. (13)).

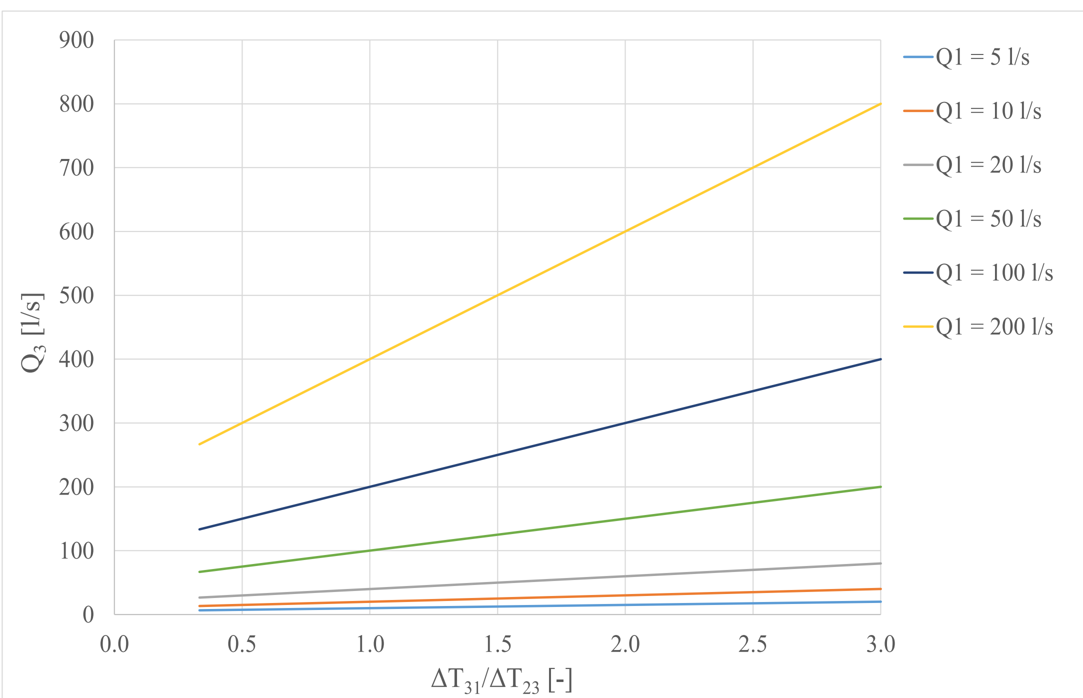

Fig. A.6. Estimation of Q_3, Scheme C (Eq. (14)).

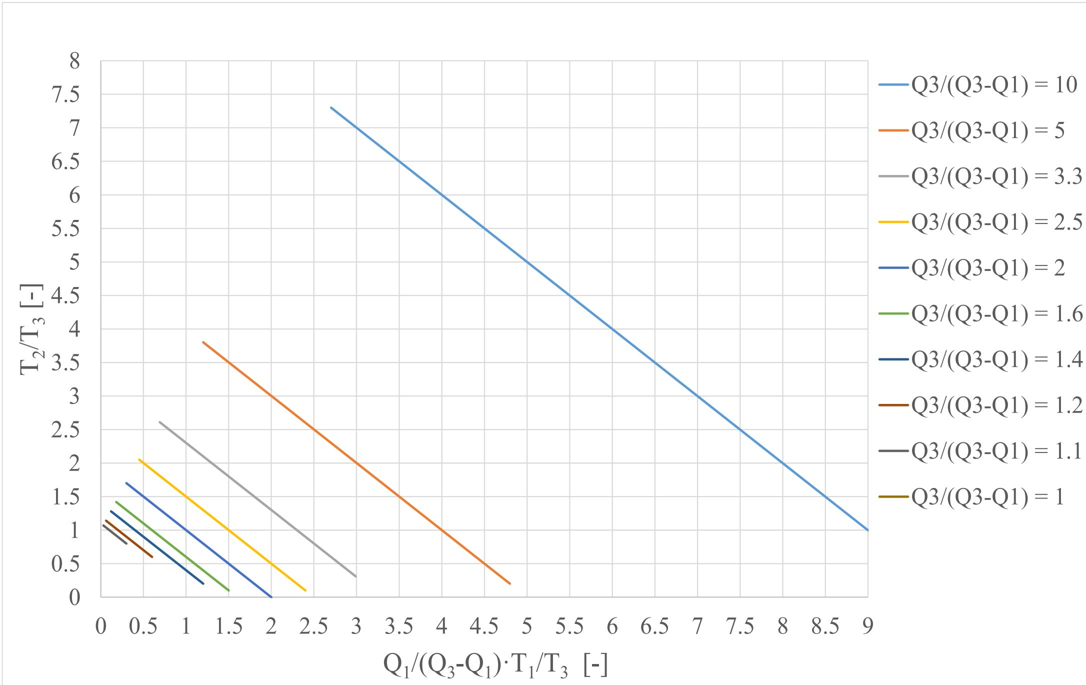

Fig. A.7. Estimation of the ratio T_2/T_3, Scheme A (Eq. (4)).

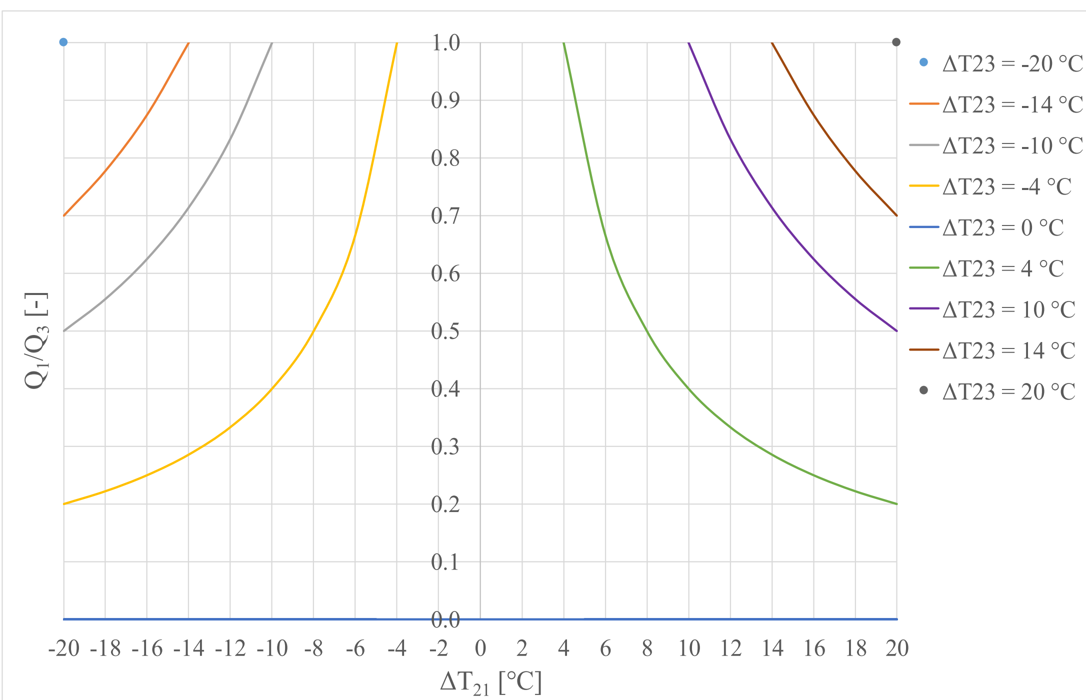

Fig. A.8. Estimation of the ratio Q_1/Q_3, Scheme B (Eq. (9)).

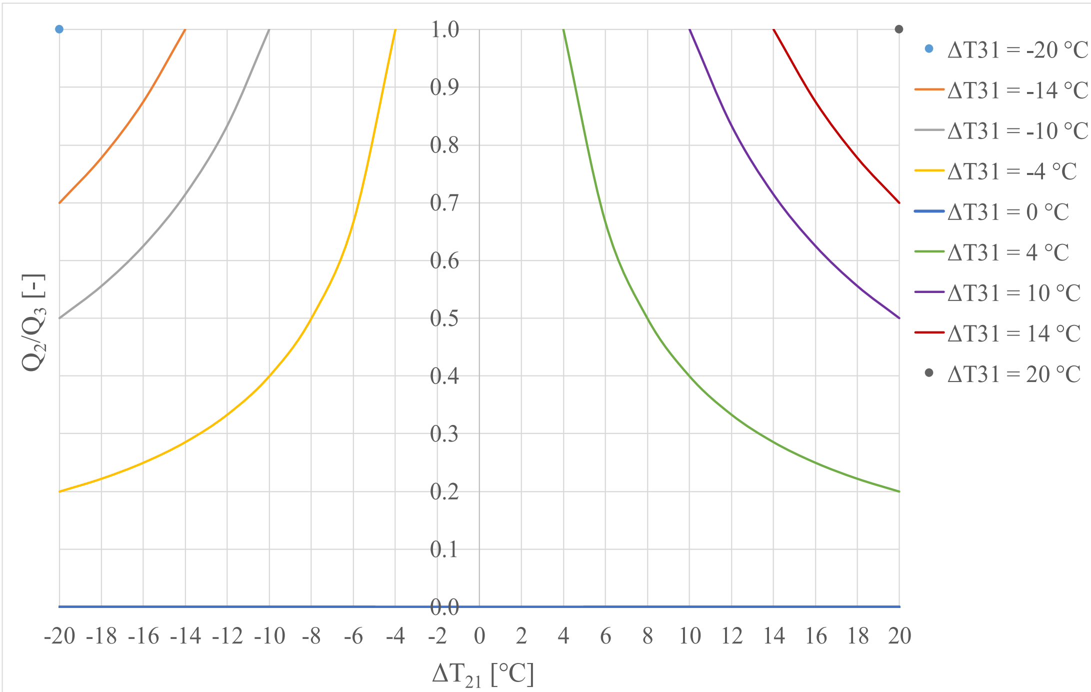

Fig. A.9. Estimation of the ratio Q_2/Q_3, Scheme B (Eq. (10)).

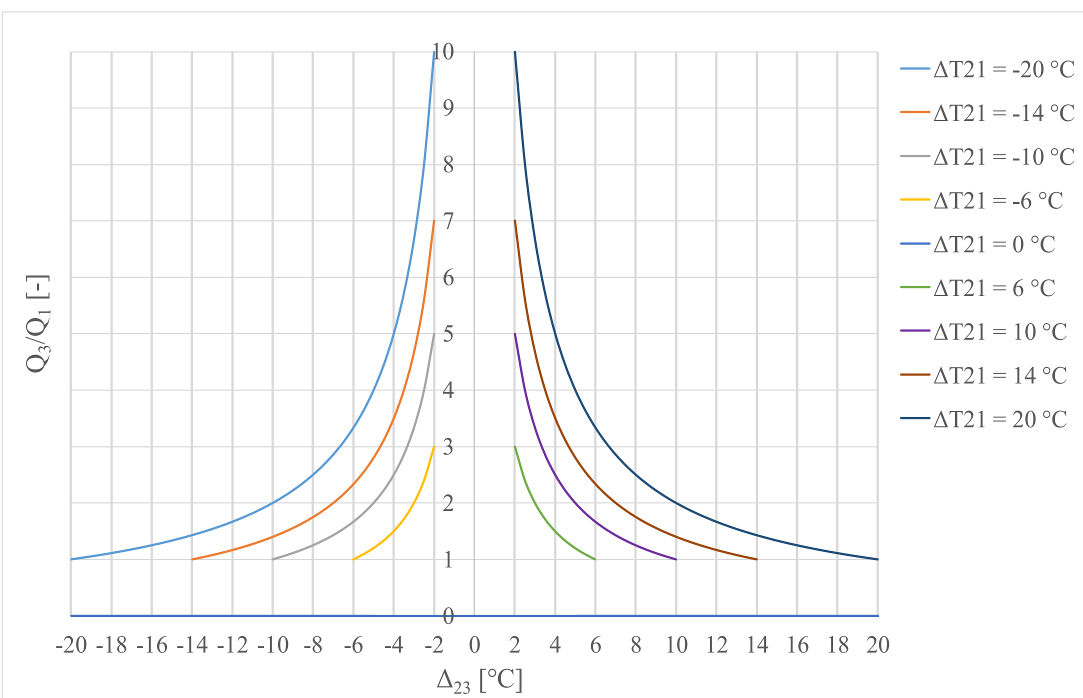

Fig. A.10. Estimation of the ratio Q_3/Q_1, Scheme C (Eq. (15)).

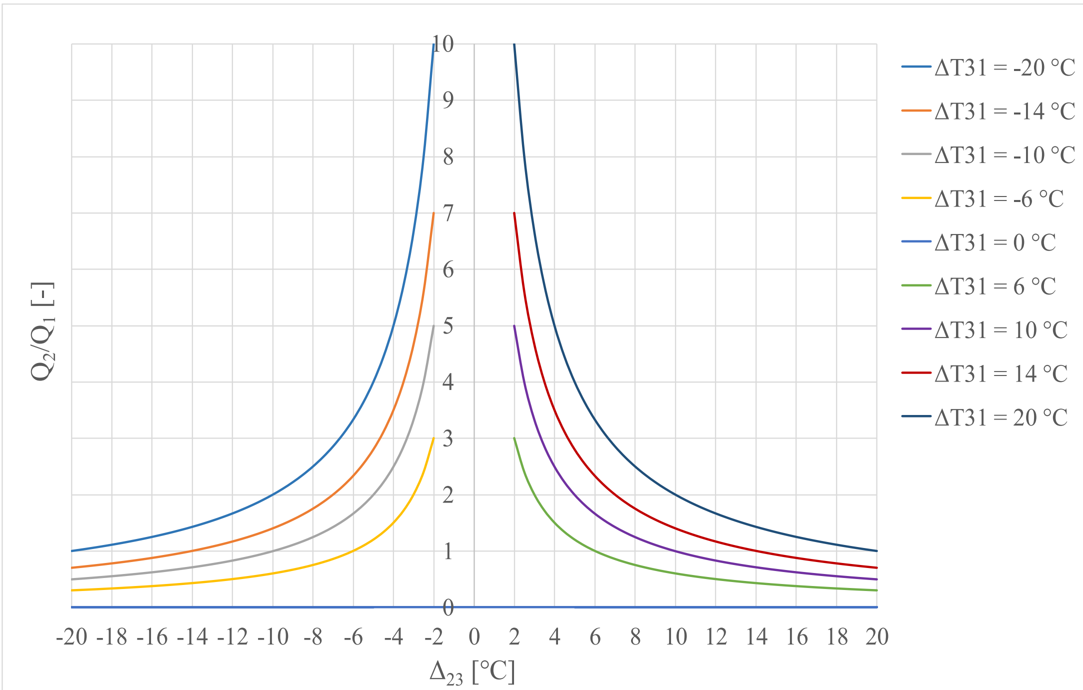

Fig. A.11. Estimation of the ratio Q_2/Q_1, Scheme C (Eq. (16)).

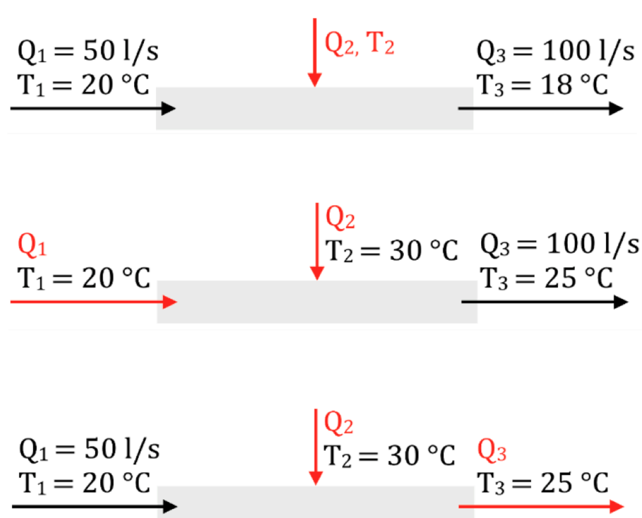

Fig. A.12. Schemes of the computational examples characterized by a balanced condition.

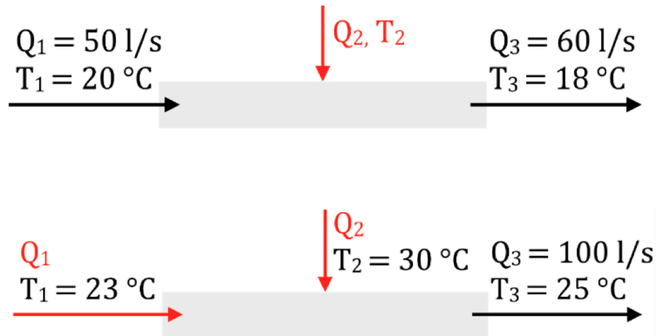

Fig. A.13. Schemes of the computational examples characterized by an unbalanced condition.

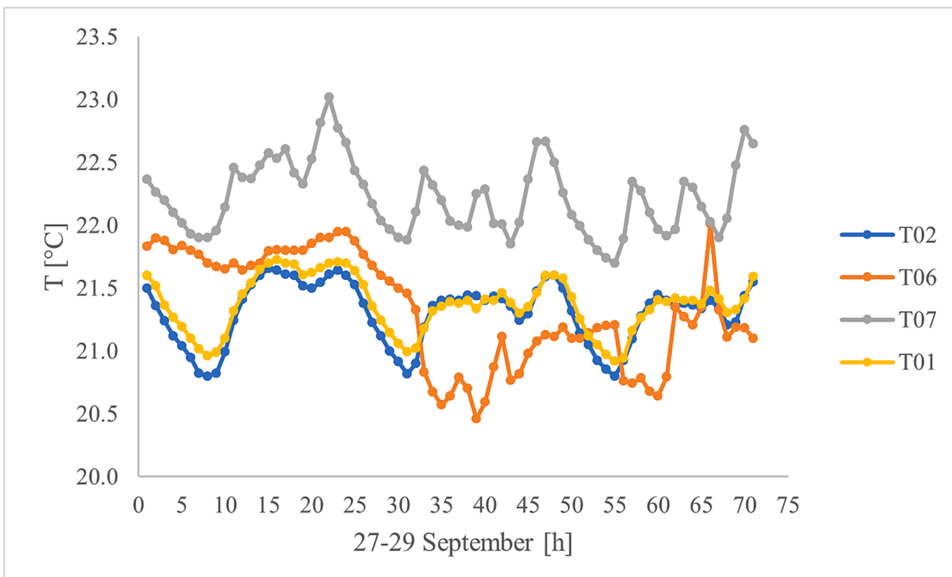

Fig. A.14. Observed temperatures in the measurements section of the Inferior Network, September 2015.

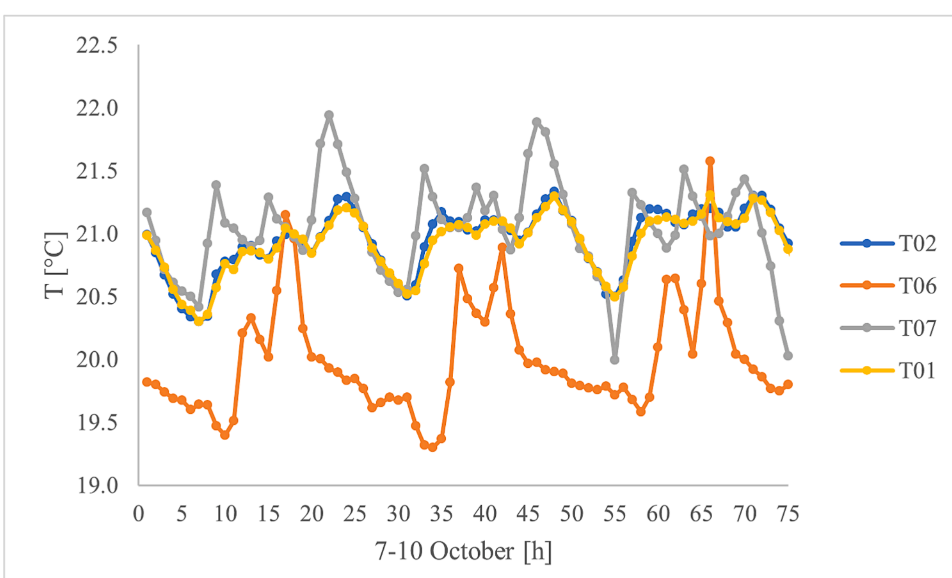

Fig. A.15. Observed temperatures in the measurements section of the Inferior Network, September 2015.

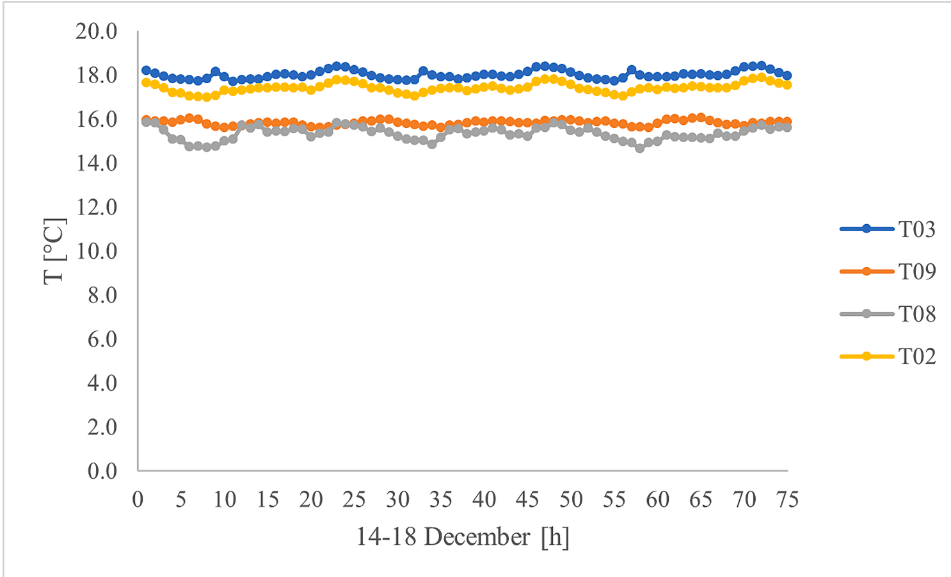

Fig. A.16. Observed temperatures in the measurements section of the Superior network, December 2015.

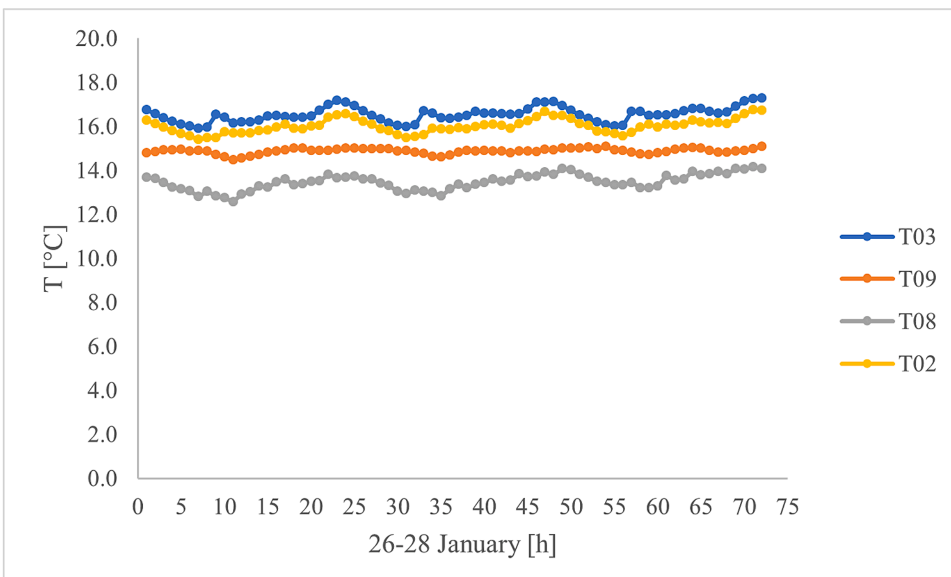

Fig. A.17. Observed temperatures in the measurements section of the Superior network, January 2016.

References

Allen, M.R., Ingram, W.J., 2002. Constraints on the future changes in climate and the hydrological cycle. Nature 419, 224–232. https://doi.org/10.1038/nature01092.

Beheshti, M., Saegrov, S., 2018. Quantification assessment of extraneous water infiltration and inflow by analysis of the thermal behaviour of the sewer network. Water 10, 1070–1087. https://doi.org/10.3390/w10081070.

Beheshti, M., Saegrov, S., 2019. Detection of extraneous water ingress into the sewer system using tandem methods - a case study in Trondheim city. Water Sci. Technol. 79, 231–239. https://doi.org/10.2166/wst.2019.057.

Bentes, I., Silva, D., Vieira, C., Matos, C., 2022. Inflow quantification in urban sewer networks. Hydrology 9 (4), 52. https://doi.org/10.3390/hydrology9040052.

Butler, D., Davies, J., 2004. Urban Drainage. CRC Press.

Camp Dresser and McKee (CDM) Inc., F.E. Jordan Associates Inc., James M. Montgomery Consulting Engineers, 1985. East Bay infiltration/inflow study manual for cost-effectiveness analysis: Oakland, CA: East Bay Municipal Utility District (EBMUD).

Choi, N., Schmidt, A.R., 2023. Rainfall-derived infiltration and inflow estimate in a sanitary sewer system using three impulse response functions derived from physics-based models. Water Resour. Manag. 37 (1), 305–319. https://doi.org/10.1007/s11269-022-03370-3.

Ellis, J.B., Bertrand-Krajewski, J.L., 2010. Assessing infiltration and exfiltration on the Performance of Urban Sewer Systems (APUSS). Water Intell. Online 9. https://doi.org/10.2166/9781780401652.

Habitat, O. N. U. 2011. Hot Cities: Battleground for Climate Change. Global Report on Human Settlement 2011.

Hausner, M.B., Kobs, S., 2016. Identifying and Correcting Step Losses in Single-Ended Fiber-Optic Distributed Temperature Sensing Data. J. Sensors, 7073619. https://doi.org/10.1155/2016/7073619.

Hoes, O.A.C., Schilperoort, R.P.S., Luxemburg, W.M.J., Clemens, F.H.L.R., Van de Giesen, N.C., 2009. Locating illicit connections in storm water sewers using fibre-optic distributed temperature sensing. Water Res. 43, 5187–5197. https://doi.org/10.1016/j.watres.2009.08.020.

Hoornweg, D., Pope, K., 2017. Population predictions for the world's largest cities in the 21st century. Environ. Urban. 29 (1), 195–216. https://doi.org/10.1177/0956247816663557.

Kechavarzi, C., Keenan, P., Xu, X., Rui, Y., 2020. Monitoring the hydraulic performance of sewers using fibre optic distributed temperature sensing. Water 12, 2451. https://doi.org/10.3390/w12092451.

Kessili, A., Vollertsen, J., Nielsen, A.H., 2018. Automated monitoring system for events detection in sewer network by distribution temperature sensing data measurement. Water Sci Technol. 78 (7), 1499–1508. https://doi.org/10.2166/wst.2018.425.

Kracht, O., Gresch, M., Gujer, W., 2007. A stable isotope approach for the quantification of sewer infiltration. Environ. Sci. Tech. 41 (16), 5839–5845. https://doi.org/10.1021/es062960c.
Lepot, M., Makris, K.F., Clemens, F.H.L.R., 2017. Detection and quantification of lateral, illicit connections and infiltration in sewers with Infra-Red camera: Conclusions after a wide experimental plan. Water Res. 122, 678–691. https://doi.org/10.1016/j.watres.2017.06.030.
Loc, H.H., Irvine, K., Chua, L., Ha, L.S., Park, E., 2022. Parameterizing Unit Hydrographs (UH) to account for Rainfall Derived Infiltration and Inflow (RDII) from different land use in tropical urban environments. J. Hydrol., 127623 https://doi.org/10.1016/j.jhydrol.2022.127623.
Lowry, C.S., Walker, J.F., Hunt, R.J., Anderson, M.P., 2007. Identifying spatial variability of groundwater discharge in a wetland stream using a distributed temperature sensor. Water Resour. Res. 43, W10408 https://doi.org/10.1029/2007WR006145.
Nguyen, H.H., Peche, A., Venohr, M., 2021. Modelling of sewer exfiltration to groundwater in urban wastewater systems: A critical review. J. Hydrol. 596, 126130 https://doi.org/10.1016/j.jhydrol.2021.126130.
Nienhuis, J., De Haan, C., Langeveld, J., Klootwijk, M., Clemens, F.H.L.R., 2013. Assessment of detection limits of fiber-optic distributed temperature sensing for detection of illicit connections. Water Sci. Technol. 67 (12), 2712–2718. https://doi.org/10.2166/wst.2013.176.
Pall, P., Allen, M., Stone, D., 2007. Testing the Clausius-Clapeyron constraint on changes in extreme precipitation under CO2 warming. Clim. Dyn. 28, 351–363. https://doi.org/10.1007/s00382-006-0180-2.
Panasiuk, O., Hedstrom, A., Marsalek, J., Ashley, R.M., Viklander, M., 2015. Contamination of storm water by wastewater: a review of detection method. J. Environ. Manag. 152, 241–250. https://doi.org/10.1016/j.jenvman.2015.01.050.
Panasiuk, O., Hedström, A., Langeveld, J., de Haan, C., Liefting, E., Schilperoort, R., Viklander, M., 2019. Using distributed temperature sensing (DTS) for locating and characterising infiltration and inflow into foul sewers before, during and after snowmelt period. Water 11, 1529. https://doi.org/10.3390/w11081529.
Pangle, L.A., Diem, J.E., Milligan, R., Adams, E., Murray, A., 2022. Contextualizing inflow and infiltration within the streamflow regime of urban watersheds. Water Resour. Res. 58 (1), e2021WR030406 https://doi.org/10.1029/2021WR030406.
Pawlowski, C.W., RheaShuster, L.L.W.D., Barden, G., Asce, M., 2014. Some factors affecting inflow and infiltration from residential sources in a core urban area: Case study in a Columbus, Ohio, neighborhood. J. Hydraul. Eng. 140 (1), 105–114. https://doi.org/10.1061/(ASCE)HY.1943-7900.0000799.
Prigiobbe, V., Giulianelli, M., 2009. Quantification of sewer system infiltration using δ 18O hydrograph separation. Water Sci. Technol. 60 (3), 727–735. https://doi.org/10.2166/wst.2009.399.
Regueiro-Picallo, M., Anta, J., Naves, A., Figueroa, A., Rieckermann, J., 2023. Towards urban drainage sediment accumulation monitoring using temperature sensors. Environ. Sci. Water Res. Technol. https://doi.org/10.1039/D2EW00820C.
Rezaee, M., Tabesh, M., 2022. Effects of inflow, infiltration, and exfiltration on water footprint increase of a sewer system: A case study of Tehran. Sustain. Cities Soc. 79, 103707 https://doi.org/10.1016/j.scs.2022.103707.
Sadeghikhah, A., Ahmed, E., Chakraborty, S., Trülzsch, S., Krebs, P., 2023. Vulnerability hotspot mapping (VHM) of sewer pipes based on deterioration factors. Urban Water J. https://doi.org/10.1080/1573062X.2023.2208107.
Sambito, M., Di Cristo, C., Freni, G., Leopardi, A., 2020. Optimal water quality sensor positioning in urban drainage systems for illicit intrusion identification. J. Hydroinf. 22 (1), 46–60. https://doi.org/10.2166/hydro.2019.036.
Schilperoort, P.S., Clemens, F.H.L.R., 2009. Fibre-optic distributed temperature sensing in combined sewer systems. Water Sci. Technol. 60 (5), 1127–1134. https://doi.org/10.2166/wst.2009.467.
Schilperoort, R.P.S., Gruber, G., Flamink, C.M.L., Clemens, F.H.L.R., Van der Graaf, J.H.M.H., 2006. Temperature and conductivity as control parameters for pollution-based real-time control. Water Sci. Technol. 54 (11–12), 257–263. https://doi.org/10.2166/wst.2006.744.
Schilperoort, R., Hoppe, H., de Haan, C., Langeveld, J., 2013. Searching for storm water inflows in foul sewers using fibre-optic distributed temperature sensing. Water Sci. Technol. 68 (8), 1723–1730. https://doi.org/10.2166/wst.2013.419.
Selker, F., Selker, J.S., 2014. Flume testing of underwater seep detection using temperature sensing on or just below the surface of sand or gravel sediments. Water Resour. Res. 50, 4530–4534. https://doi.org/10.1002/2014WR015257.
Selker, J.S., Thévenaz, L., Huwald, H., Mallet, A., Luxemburg, W., van de Giesen, N., Stejskal, M., Zeman, J., Westhoff, M., Parlange, M.B., 2006. Distributed fiber-optic temperature sensing for hydrologic systems. Water Resour. Res. 42 (12) https://doi.org/10.1029/2006WR005326.
Shi, B., Catsamas, S., Deletic, B., Wang, M., Bach, P.M., Lintern, A., Deletic, A., McCarthy, D.T., 2022. Illicit discharge detection in stormwater drains using an Arduino-based low-cost sensor network. Water Sci. Technol. 85 (5), 1372–1383. https://doi.org/10.2166/wst.2022.034.
Tanda, M.G., D'Oria, M., Secci, D., Todaro, V., 2023. Identification of the inflow source in a foul sewer system through techniques of inverse modelling. J. Phys.: Conf. Series 2444 (1), 012011. https://doi.org/10.1088/1742-6596/2444/1/012011.
Tyler, S.W., Selker, J.S., Hausner, M.B., Hatch, C.E., Torgersen, T., Thodal, C.E., Schladow, S.G., 2009. Environmental temperature sensing using Raman spectra DTS fiber-optic methods. Water Resour. Res. 45, W00D23 https://doi.org/10.1029/2008WR007052.
Ukil, A., Braendle, H., Krippner, P., 2012. Distributed temperature sensing: review of technology and applications. IEEE Sens. J. 12 (5), 885–892. https://doi.org/10.1109/JSEN.2011.2162060.
Van de Giesen, N., Steele-Dunne, S.C., Jansen, J., Hoes, O., Hausner, M.B., Tyler, S., Selker, J., 2012. Double-ended calibration of fiber-optic Raman spectra distributed temperature sensing data. Sensors (Basel). 12 (5), 5471–5485. https://doi.org/10.3390/s120505471.
Vosse, M., Schilperoort, R., de Haan, C., Nienhuis, J., Tirion, M., Langeveld, J., 2013. Processing of DTS monitoring results: automated detection of illicit connections. Water Pract. Technol. 8 (3–4), 375–381. https://doi.org/10.2166/wpt.2013.037.
Weiß, G., Brombach, H., Haller, B., 2002. Infiltration and inflow in combined sewer systems: Long-term analysis. Water Sci. Technol. 45 (7), 11–19. https://doi.org/10.2166/wst.2002.0112.
Xu, Z., Qu, Y., Wang, S., Chu, W., 2021. Diagnosis of pipe illicit connections and damaged points in urban stormwater system using an inversed optimization model. J. Clean. Prod. 292 (552), 126011 https://doi.org/10.1016/j.jclepro.2021.126011.
Xu, C., Xu, Z., Chu, W., Wu, S., Xiao, R., Su, L., 2023. Identification of high oxygen-consuming substances in stormwater drainage systems illicitly connected with sewage system. J. Environ. Sci. 138, 132–140. https://doi.org/10.1016/j.jes.2023.03.033.
Zhang, M., Liu, Y., Cheng, X., Zhu, D.Z., Shi, H., Yuan, Z., 2018. Quantifying rainfall-derived inflow and infiltration in sanitary sewer systems based on conductivity monitoring. J. Hydrol. 558, 174–183. https://doi.org/10.1016/j.jhydrol.2018.01.002.
Zhang, K., Parolari, A.J., 2022. Impact of stormwater infiltration on rainfall-derived inflow and infiltration: A physically based surface–subsurface urban hydrologic model. J. Hydrol. 610, 127938 https://doi.org/10.1016/j.jhydrol.2022.127938.
Zhang, K., Sebo, S., McDonald, W., Bhaskar, A., Shuster, W., Stewart, R.D., Parolari, A.J., 2023. The role of inflow and infiltration (I/I) in urban water balances and streamflow regimes: A hydrograph analysis along the sewershed-watershed continuum. Water Resour. Res. 59 (4) https://doi.org/10.1029/2022WR032529.
Zhao, Z., Yin, H., Xu, Z., Peng, J., Yu, Z., 2020. Pin-pointing groundwater infiltration into urban sewers using chemical tracer in conjunction with physically based optimization model. Water Res. 175, 115689 https://doi.org/10.1016/j.watres.2020.115689.